Kinetic Insight into the Effect of Self-Generated CO2 on the Thermal Decomposition of Inorganic Carbonates in an Inert Gas Atmosphere: ZnCO3 and CaCO3

Mito Hotta, Loïc Favergeon, Nobuyoshi Koga

Kinetic Insight into the Effect of Self-Generated CO_2 on the Thermal Decomposition of Inorganic Carbonates in Inert Gas Atmosphere: $ZnCO_3$ and $CaCO_3$

Mito Hotta,[1] Loic Favergeon,[2] and Nobuyoshi Koga[1,]*

[1] Department of Science Education, Division of Educational Sciences, Graduate School of Humanities and Social Sciences, Hiroshima University, 1-1-1 Kagamiyama, Higashi-Hiroshima 739-8524, Japan
[2] Mines Saint-Etienne, Univ. Lyon, CNRS, UMR 5307 LGF, Centre SPIN, F-42023 Saint-Etienne, France

Abstract

This study aims to parameterize the effect of self-generated gas on the thermal decomposition of inorganic solids in an inert gas atmosphere. The kinetics of reversible thermal decomposition should be described as a function of the temperature and partial pressure of gaseous product in the reaction atmosphere; however, the partial pressure of evolved gas at the specific reaction site is difficult to measure because of the heterogeneous reaction nature. Extrapolation of the universal kinetic relationship established over different temperatures and partial pressure of the gaseous product in the reaction atmosphere to a reaction condition in an inert gas atmosphere is proposed as a possible method for estimating the effect of self-generated gas on such reactions in an inert gas atmosphere. This idea was practically demonstrated, as exemplified by the thermal decomposition of $ZnCO_3$ and $CaCO_3$ in a stream of dry N_2 and air. By setting the effective partial pressure of CO_2 ($p(CO_2)$) as a weighted sum of the atmospheric and self-generated $p(CO_2)$, a universal kinetic description of these thermal decomposition reactions across different temperatures and $p(CO_2)$ values including those in an inert gas atmosphere was achieved, and the contribution of self-generated $p(CO_2)$ was parameterized. Furthermore, the change in the contribution of self-generated $p(CO_2)$ as the reaction advanced was evaluated using consecutive surface and phase boundary-controlled reaction models. The proposed kinetic analysis approach addresses many issues in the conventional kinetic analysis approach and provides detailed kinetic insight into the reversible thermal decomposition of solids.

1. Introduction

The reversible thermal decomposition of inorganic solids has been used for various industrial and technological applications and has significantly contributed to promoting civilization in history. These old reaction systems have been attracting significant attention for solving today's global issues related to energy supply and environmental protection.[1-10] For example, such reversible systems, comprising the endothermic thermal decomposition and exothermic solid–gas reactions, are promising for developing environmentally friendly technology of thermochemical energy storage. Solid–gas reactions can be used to absorb unwanted gaseous species to protect the environment, whereas thermal decomposition reproduces the solid absorbent.[1-5] Furthermore, the reversible exothermic and endothermic processes construct an energy storage scheme. A reversible reaction system can also be useful for the storage and release of fuel such as hydrogen.[6-10] Therefore, a detailed kinetic understanding of both reaction

processes is essential to realize the future technologies of energy storage and environmental protection. Such reversible reaction systems include the thermal decomposition of metal carbonate and the reaction between metal oxide and CO_2, as typically seen for the thermal decomposition of $CaCO_3$ and the reaction between CaO and CO_2 (Ca-looping system).[1-5, 11-17] The kinetics of both forward and reverse processes have been extensively studied for practical applications. [18-26] In particular, kinetic study on the thermal decomposition of $CaCO_3$ has a long history and is one of the most extensively studied systems in this class of reaction.[27-40] The reaction is characterized by heterogenous constraints and the significant effect of atmospheric CO_2. Thus, the kinetics varies with temperature (T), partial pressure of CO_2 ($p(CO_2)$) with reference to the equilibrium CO_2 pressure of the reaction ($P_{eq}(T)$), and the advancement of the reaction characterized by the degree of reaction (α). Therefore, the basic kinetic equation can be expressed as follows: [30, 33, 41-47]

$$\frac{d\alpha}{dt} = A\exp\left(-\frac{E_a}{RT}\right) f(\alpha) h(p(CO_2), P_{eq}(T)), \quad (1)$$

where A, E_a, and R denote the Arrhenius preexponential factor, apparent activation energy, and gas constant, respectively. The function, $f(\alpha)$, denotes the kinetic model function for describing the changes in the reaction rate as the reaction advances under isothermal conditions. In addition, $h(p(CO_2), P_{eq}(T))$ denotes the accommodation function (AF) for describing the change in the reaction rate by $p(CO_2)$ and $P_{eq}(T)$ values. Various functional forms of AF have been proposed to satisfy the universal kinetic description of the subjected thermal decomposition process.[47-48] Recently, an analytical form of AF has been proposed for universally describing the reversible thermal decomposition of solids and has been tested with various reaction systems. [40, 49-59]

$$h(p(CO_2), P_{eq}(T)) = \left(\frac{1}{p(CO_2)}\right)^a \left[1 - \left(\frac{p(CO_2)}{P_{eq}(T)}\right)^b\right], \quad (2)$$

where the exponents (a, b) are variables and optimized through kinetic calculations to enable a universal kinetic description under various temperature and $p(CO_2)$ conditions. The AF in eq. (2) has been derived based on the theoretical consideration of the elementary steps of surface and interface reactions by selecting one possible rate-determining step with a steady-state approximation for the other elementary steps.[40, 49, 51-53, 59] When (a, b) = (0, 1), eq. (2) becomes identical to the traditional and most widely used AF, i.e. $h(p(CO_2), P_{eq}(T))=1-p(CO_2)/P_{eq}(T)$.[30, 33, 41-45] In addition, most of the previously proposed AF can be expressed using eq. (2) with individual specific values of (a, b). The formulation of eq. (2) is outlined in the Supporting Information (section S1, Table S1). We have previously demonstrated that the thermal decomposition of $CaCO_3$ under various temperature and atmospheric $p(CO_2)$ conditions can be universally described using eqs. (1) and (2).[40, 56-57] For a more detailed kinetic description, the effect of self-generated CO_2 by the reaction should be considered in the kinetic equation. When the contributions of atmospheric CO_2 and self-generated CO_2 to the decomposition kinetics were empirically expressed as a linear combination, the universal kinetic relationships established based on eqs. (1) and (2) were significantly improved, providing the contributions of respective CO_2 sources and their changes as the reaction advanced.[40]

Further concern on the kinetics of the reversible thermal decomposition of solids is the effect of self-generated gas on the reaction in an inert gas atmosphere. In many previous studies on the reversible thermal decomposition of solids, significant efforts have been made to diminish the effects of selfgenerated gas on the kinetics by reducing the sample mass (m_0) and heating rate (β), as well as increasing the flow rate (q_v) of inert gas to purge the evolved gas from the reaction system. If successful, the kinetic equation can be simplified to a basic kinetic equation for a single-step reaction by ignoring AF in eq. (1).[59-62]

$$\frac{d\alpha}{dt} = A\exp\left(-\frac{E_a}{RT}\right)f(\alpha) \qquad (3)$$

However, the simplified kinetic approach based on eq. (3) occasionally generates issues in interpreting the kinetics based on physical chemistry. These issues include the variation of the Arrhenius parameters with experimental conditions such as m_0, β, and q_v of inert gas.[63-64] In the case of the thermal decomposition of $CaCO_3$, the ideal kinetic relationship of eq. (3) is easily broken by a small change in the sample mass, even in a low-pressure atmosphere and at a slow rate of gaseous evolution.[35] For the reversible thermal decomposition of solids, the experimental settings for reducing $p(CO_2)$ in the reaction system, i.e., smaller m_0, slower β, larger q_v of inert gas, and lower atmospheric pressure, generally reduce the reaction temperature. The lowering of the reaction temperature is always accompanied by a decrease in the evolution rate of CO_2 and $P_{eq}(T)$ value. Therefore, the ratio of self-generated $p(CO_2)$ ($p(CO_2)_{SG}$) and $P_{eq}(T)$ exhibits a limited change by any attempt to reduce $p(CO_2)$ in the reaction system. In this study, we propose considering the effect of self-generated CO_2 on the thermal decomposition of metal carbonates in an atmosphere with a negligible CO_2 concentration as an alternative kinetic approach to well-studied reversible thermal decomposition processes. For this purpose, the thermal decomposition of two metal carbonates, i.e., $ZnCO_3$ and $CaCO_3$, were selected as model processes, because the effect of atmospheric CO_2 has been well described using eqs. (1) and (2), where a more significant effect of CO_2 has been observed for $CaCO_3$.[40, 53]

$$ZnCO_3(s) \rightleftharpoons ZnO(s) + CO_2(g) \qquad (4)$$

$$(\Delta_r H^\circ_{625} = 66.7\ \text{kJ})$$

$$CaCO_3(s) \rightleftharpoons CaO(s) + CO_2(g) \qquad (5)$$

$$(\Delta_r H^\circ_{900} = 171.4\ \text{kJ})$$

Initially, the results of the conventional kinetic approach based on eq. (3) are demonstrated for both reactions in a stream of dry N_2 gas and air to overview the effect of self-generated CO_2. Then, with reference to the previously established universal kinetic description under various temperatures and atmospheric $p(CO_2)$ ($p(CO_2)_{ATM}$) conditions for individual reactions, the effect of self-generated CO_2 on the reactions in a stream of dry N_2 or air is parameterized using eqs. (1) and (2) with an empirical expression of the effective $p(CO_2)$ as a weighted sum of the atmospheric $p(CO_2)_{ATM}$ and self-generated $p(CO_2)_{SG}$. The kinetic approach is further extended to the physico-geometrical kinetic description for the consecutive surface reaction (SR) and

subsequent phase boundary-controlled reaction (PBR),[65-66] through which the changes in the effect of self-generated CO_2 as the physico-geometrical reaction step advanced from surface reaction to phase boundary-controlled reaction are evaluated.

2. Experimental

2.1 Sample description

$ZnCO_3$ was prepared in our laboratory by hydrothermal treatment of precipitated hydrozincite in a $NaHCO_3$ solution. The preparation and characterization have been described in detail in our previous article. [53] $CaCO_3$ was purchased from Fujifilm-Wako Pure Chem. Co. (> 99.9%), which was also used in our previous study that focused on the kinetics of thermal decomposition at various atmospheric $p(CO_2)$ values[40] and the effect of atmospheric water vapor on the kinetics.[39] Characterizations for the $ZnCO_3$ and CaCO3 samples used in this study are summarized in section S2 in Supporting Information (Figure S1).

2.2 Influences of measurement conditions on the thermoanalytical curves

The thermal decomposition of $ZnCO_3$ and $CaCO_3$ was traced using a thermogravimetry (TG)–differential thermal analysis (DTA) system (TG-8121, Thermoplus Evo2 system, Rigaku) equipped with a CO_2 concentration meter (LX-720 (0–5000 ppm), IIJIMA) for detecting CO_2 evolution. The sampling was performed in a Pt pan (diameter: 5 mm; depth: 2.5 mm) with varying $m0$ in the range of 0.5–10 mg. TG–derivative TG (DTG)–DTA curves and the CO_2 concentration ($c(CO_2)$) in the outlet gas from the instrument (evolved gas analysis (EGA)) were simultaneously recorded by linearly heating the sample at a β of 5 K min^{-1} in a stream of dry N2 gas ($p(H_2O)$ < 0.2 kPa) at a qv of 300 cm^3 min^{-1}. The scanning temperature ranges for the TG–DTG–DTA–EGA($c(CO_2)$) measurements for the $ZnCO_3$ and $CaCO_3$ samples were 300 K–873 K and 573 K–1173 K, respectively. Under the same heating conditions (β = 5 K min^{-1}), the TG–DTG–EGA($c(CO_2)$) curves for $ZnCO_3$ of 3.0 mg or $CaCO_3$ of 2.5 mg were also recorded by varying the q_v value in the range of 50–500 cm^3 min^{-1}.

2.3 Measurements of kinetic data

TG–DTG–EGA(c(CO2)) curves for the thermal decomposition of $ZnCO_3$ of 3.0 mg or $CaCO_3$ of 2.5 mg were recorded under different heating conditions of isothermal, linear nonisothermal, and controlled transformation thermal analysis (CRTA) [67-68] modes in a stream of dry N_2 ($p(H_2O)$ < 0.2 kPa) or air ($p(H_2O)$ < 0.2 kPa) at a qv of 300 cm^3 min^{-1}. For the measurements in an isothermal heating mode, the sample was initially heated to a programmed temperature at a β of 10 K min^{-1} and maintained at that temperature until the thermal decomposition process is completed. A series of TG–DTG–EGA($c(CO_2)$) curves were systematically recorded by varying the programmed constant temperature: $534 \leq T/K \leq 578$ and $553 \leq T/K \leq 590$ for the thermal decomposition of $ZnCO_3$ in a stream of dry N_2 and air, respectively; $805 \leq T/K \leq 833$ and $845 \leq T/K \leq 872$ for the thermal decomposition of $CaCO_3$ in a stream of dry N_2 and air, respectively. The TG–DTG–EGA($c(CO_2)$) curves for these thermal decomposition processes under linear nonisothermal conditions were systematically recorded at different β values ($0.5 \leq \beta$ / K $min^{-1} \leq 10$): scanning temperature ranges for the thermal decomposition of $ZnCO^3$ in a stream of dry N_2 and air were 423 K–823 K and 473 K–873 K, respectively; those for the thermal decomposition of $CaCO_3$ in both a stream of dry N_2 and air were 573 K–1173 K. In the measurements under CRTA modes, the sample was linearly heated at a β of 2 K min^{-1}, whereas, during the thermal decomposition process, the mass loss rate was regulated to be different constant values (C) in the ranges of 3–18 μg min^{-1} and 2.5–15 μg min^{-1} for the $ZnCO_3$ and

$CaCO_3$ samples, respectively. The TG–DTA instrument was calibrated prior to the sample measurements regarding the measured temperature and mass change value using standard methods.[69] The sample temperature was calibrated using the DTA signal for the melting of Ga, In, Sn, Pb, Zn, Al, and Ag (purity ≥ 99.99%, Nilaco) at a β of 5 K min^{-1} in a stream of dry N_2 (qv = 300 cm^3 min^{-1}), whereas the mass change value was calibrated using a standard weight of 2.00 mg and further validated using mass loss curves for the thermal decomposition of $CaC_2O_4 \cdot H_2O$ (m_0 = 5.0 mg, ≥ 99.9985%, Alfa Aesar) recorded by heating linearly at a β of 5 K min^{-1} in a stream of dry N_2 (qv = 300 cm^3 min^{-1}). The CO_2 meter was also calibrated using standard gas of N_2 (≥ 99.999%) and N_2–CO_2 mixed gas ($c(CO_2)$: 4000 ppm).

3. Results and Discussion

3.1 Influence of experimental factors

Figure S2 depicts the TG–DTG–EGA($c(CO_2)$) curves for the thermal decomposition of $ZnCO_3$ and $CaCO_3$ with different m_0 values recorded under linear nonisothermal conditions at a fixed β of 5 K min^{-1} in a stream of dry N_2 gas at a fixed qv of 300 cm^3 min^{-1}. The thermoanalytical (TA) curves for both samples shifted systematically to higher temperatures as the m_0 value increased, indicating that the TA curves were reflected by the reaction behavior of the sample assemblage rather than each sample particle. For the thermal decomposition of $ZnCO_3$ (Figure S2(a)), the reaction initiation temperature detected by TG and DTG curves was practically invariant irrespective of m_0, and the shift of the TG and DTG curves to higher temperatures became more significant as the reaction advanced. An increase in the thickness of the sample bed can be one of the causes of the temperature shift when the reaction is constrained geometrically, characterized by the initiation at the top surface of the sample bed and the advancement of the reaction interface toward the bottom.[63, 70-71] The EGA($c(CO_2)$) of the outlet gas from the reaction chamber exhibited a smooth peak during the reaction, and the peak height increased systematically as m_0 value increased. Note that the measured $c(CO_2)$ value is associated with the evolution rate of CO_2, although the actual $c(CO_2)$ value in the sample pan has been diluted by the dry N_2 gas flowing at a fixed qv. No matter, it is expected that the $p(CO_2)$ value in the sample matrix and pan is larger during the reaction of the sample with a larger m_0 value. The effect of self-generated CO_2 on the kinetics of the reaction is also a possible cause of the shift of TA curves to higher temperatures as the m0 value increased. In the case of the thermal decomposition of $CaCO_3$ (Figure S2(b)), the shift of TA curves with increasing m0 was more obvious than that of $ZnCO_3$. The shift of the reaction initiation temperature to higher temperatures with increasing m0 value was specifically observed for the thermal decomposition of $CaCO_3$. Because the phenomenon cannot be explained by the geometrical constraints owing to the sample bed, the effect of self-generated CO_2 on the SR in the early stage of the reaction may be one of the possible causes of the initiation temperature shift. Figure S3 shows the variations of TG–DTG–EGA($c(CO_2)$) curves by the effect of the qv of dry N_2 gas. The CO_2 concentration in the outlet gas during the thermal decomposition process increased as the qv value decreased in both reactions because the evolved CO_2 is diluted by the flowing dry N_2 gas. This implies that decreasing the q_v value increases the CO_2 concentration retained in the sample pan. For the thermal decomposition of $ZnCO_3$ (Figure S3(a)), the shift of the TA curves with q_v did not occur systematically. This can be interpreted as the cooling effect of the reaction system increasing with increasing q_v value, in addition to the retardation effect of CO_2. Conversely, the TA curves for the thermal decomposition of $CaCO_3$ shifted systematically to higher temperatures as the q_v value decreased (Figure S3(b)). Therefore, it was expected that the retardation effect caused by the retained CO_2 in the sample pan was more significant for the

thermal decomposition of CaCO3. Figure 1 compares the TG–DTG–EGA($c(CO_2)$) curves recorded in a stream of dry N_2 and air (q_v = 300 cm^3 min^{-1}) for individual reactions. For the thermal decomposition of $ZnCO_3$ (Figure 1(a)), a slight retardation of the reaction initiation temperature in air was detected. However, the TG and DTG curves for the subsequent reaction were practically invariant between the dry N_2 and air atmospheres. A more significant retardation in the entire reaction process, including the reaction initiation temperature, was observed for the thermal decomposition of $CaCO_3$ in air as a shift of the reaction temperature to higher temperatures (Figure 1(b)). Thus, the thermal decomposition of $CaCO_3$ is sensitive to a slight increase in $c(CO_2)$, i.e., ca. 500 ppm. Under the conditions of a larger m_0, smaller qv, and larger β, the increase in $c(CO_2)$ retained in the sample pan during the majority of the reaction in a stream of dry N_2 gas is expected to exceed the difference in $c(CO_2)$ in dry N_2 and air, indicating that the thermal decomposition of $CaCO_3$ in a stream of dry N_2 gas is influenced by the self-generated CO_2.

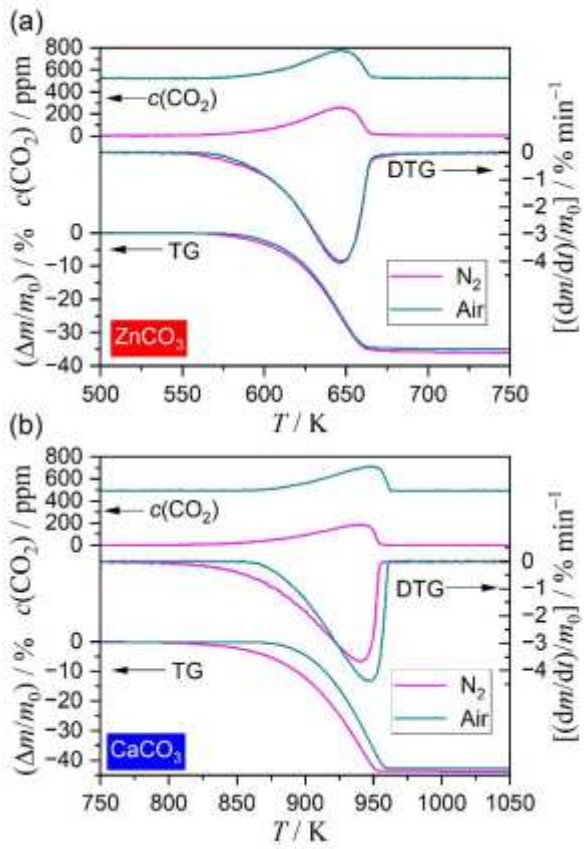

Figure 1. Comparison of TG–DTG–EGA($c(CO_2)$) curves recorded at a β of 5 K min^{-1} in a stream of dry N_2 and air (q_v = 300 cm^3 min^{-1}) for individual reactions of (a) $ZnCO_3$ ($m_0 \approx 2.93$ mg) and (b) $CaCO_3$ ($m_0 \approx 2.50$ mg).

Based on the preliminary TG–DTG–EGA($c(CO_2)$) measurements under different measurement conditions (Figures 1, S2, and S3), the m_0 values of 3.0 and 2.5 mg were selected for the thermal decomposition of $ZnCO_3$ and $CaCO_3$, respectively, to record the kinetic curves of the individual thermal decomposition processes. The q_v value was fixed as 300 cm^3 min^{-1} under both conditions of a stream of dry N_2 and air. Notably, these measurement conditions were selected as the best to reduce the effect of self-generated CO_2 on the thermal decomposition processes

by minimizing the thickness of sample bed and maximizing the purge efficiency of the evolved CO_2 during the reactions, while maintaining the stability and reproducibility of the measured thermoanalytical curves. Figure 2 shows the TG–DTG– EGA($c(CO_2)$) curves under isothermal and linear nonisothermal conditions and TG–temperature profile– EGA($c(CO_2)$) curves under CRTA conditions for the thermal decomposition of $ZnCO_3$ in a stream of dry N_2 and air. The same for $CaCO_3$ is shown in Figure 3. In both reactions, irrespective of the atmospheric condition, the TA curves systematically shifted with changes in the heating parameters (T, β, and C) in the respective heating modes. Notably, the EGA($c(CO_2)$) signal is proportional to the corresponding DTG signal and systematically increased with increasing T, β, and C. In the general kinetic approach to the thermal decomposition of solids based on the basic kinetic equation (eq. (3)) without considering the effect of self-generated gas, it is recommended to use a series of TA curves recorded at different heating parameters in the kinetic calculation to obtain reliable results.[60] However, in a strict sense, this approach is successful only when the effect of the self-generated reaction environment caused by the evolved gas and the enthalpy change of the reaction, as well as changes in the self-generated reaction environment with the heating parameters, are negligible. Comparing the TA curves recorded in a stream of dry N_2 and air, the larger retardation effect of CO_2 in air (approximately 500 ppm) was observed for the thermal decomposition of $CaCO_3$ in all heating program modes. Notably, no evidence of the induction period was observed in both reactions under isothermal conditions even though the thermal decomposition of $CaCO_3$ exhibited an obvious induction period at higher atmospheric $p(CO_2)$ values. [40] For each TG–DTG curve, α and its time derivative ($d\alpha/dt$) were calculated with reference to the total mass loss values observed in each TG curve.

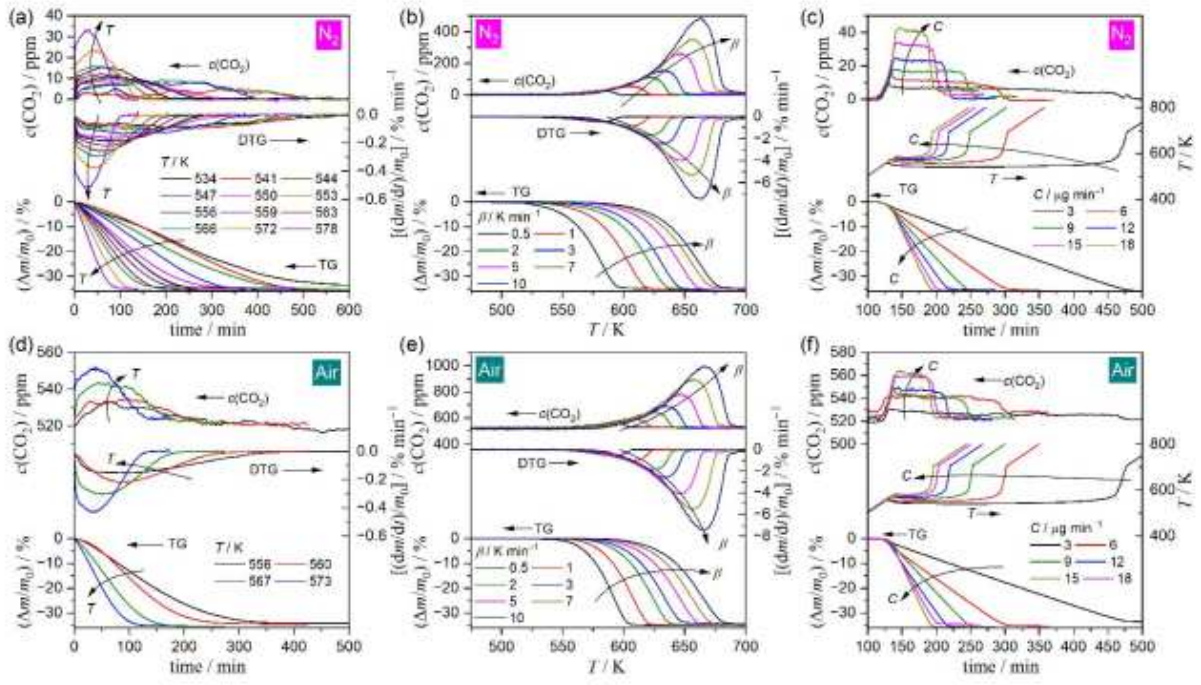

Figure 2. TG–DTG–EGA($c(CO_2)$) or TG–temperature profile–EGA($c(CO_2)$) curves for thermal decomposition of $ZnCO_3$ in a stream of dry N_2 gas ((a)–(c)) or air ((d)–(f)) (q_v = 300 cm_3 min_{-1}) under different heating modes: (a) isothermal (m_0 = 3.01 ± 0.10 mg), (b) nonisothermal (m_0 = 3.04 ± 0.09 mg), (c) CRTA (m_0 = 3.01 ± 0.03 mg), (d) isothermal (m_0 = 2.94 ± 0.06 mg), (e) nonisothermal (m_0 = 2.98 ± 0.08 mg), and (f) CRTA (m_0 = 2.99 ± 0.02 mg).

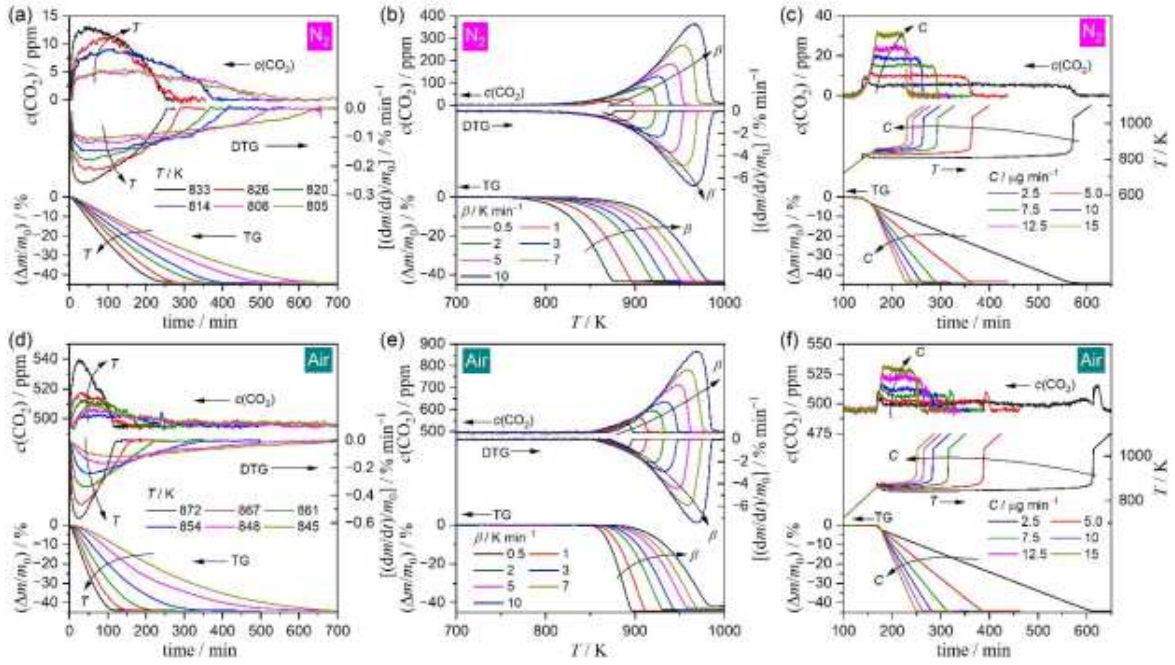

Figure 3. TG–DTG–EGA(c(CO2)) or TG–temperature profile–EGA(c(CO2)) curves for thermal decomposition of CaCO3 in a stream of dry N2 gas ((a)–(c)) or air ((d)–(f)) (q_v = 300 cm3 min-1) under different heating modes: (a) (m_0 = 2.52 ± 0.02 mg), (b) (m_0 = 2.56 ± 0.09 mg), (c) (m_0 = 2.50 ± 0.05 mg), (d) (m_0 = 2.50 ± 0.03 mg), (e) (m_0 = 2.48 ± 0.06 mg), and (f) (m_0 = 2.52 ± 0.02 mg).

3.2 Formal kinetic analysis

The basic kinetic equation for the single-step reaction (eq. (3)) was primarily assumed to analyze the series of kinetic curves composed of data points (time (t), temperature (T), α, dα/dt): [59, 61-62, 72] The logarithmic form of the kinetic equation is expressed as follows

$$\ln\left(\frac{\mathrm{d}\alpha}{\mathrm{d}t}\right) = \ln[Af(\alpha)] - \frac{E_\mathrm{a}}{RT} \qquad (6)$$

Based on eq. (6), the kinetic relationships can be described in the three-dimensional (3D) coordinate of (T-1, α, ln (dα/dt)).[59] The kinetic data obtained by the systematic TG measurements (Figures 2 and 3) covered a curved surface in the 3D kinetic coordinate in both the thermal decomposition processes of ZnCO3 and CaCO3 under each atmospheric condition (Figures S4 and S5). The formal kinetics was characterized in a stepwise manner by analyzing the isoconversional relationship that appeared on the plane perpendicular to the α axis in the 3D coordinate and then the isothermal relationship that appeared on the plane perpendicular to the T-1 axis. Figures 4 and 5 show the results of formal kinetic analysis for the thermal decomposition of ZnCO3 and CaCO3, respectively. The isoconversional relationship was examined using the Friedman plot of ln (dα/dt) versus T-1 at various selected α values[73] (Figures S6 and S7). For the thermal decomposition of ZnCO3, the data points at a selected α value formed the respective straight lines for the reactions in a stream of dry N2 and air (Figures 4(a)

and S6), with detectable deviation of the data points from the straight line for the reactions under isothermal conditions in a stream of air. This caused a slightly larger slope of the entire Friedman plot for the reaction in a stream of air. In the thermal decomposition of $CaCO_3$, the Friedman plots at a selected α exhibited significantly different slopes for the reactions in a stream of dry N_2 and air (Figure 5(a)), with a larger slope observed for the reaction in a stream of air. Irrespective of α, an ideal linear correlation was observed for the reaction in a stream of dry N_2; meanwhile, in a stream of air, a curved plot with a convex shape was detected (Figures 5(a) and S7). In both reactions, irrespective of the atmospheric condition, the E_a values calculated from the slope of the Friedman plots were approximately constant during the reactions (Figures 4(b) and 5(b)). For the thermal decomposition of $ZnCO_3$, slightly larger E_a values were obtained for the reaction in a stream of air (Figure 4(b)). The same trend of the difference in the E_a values in a stream of dry N_2 and air was observed for the thermal decomposition of $CaCO_3$ (Figure 5(b)); however, the difference in the E_a values was significantly larger than that for the thermal decomposition of $ZnCO_3$. The average E_a values for each reaction under individual atmospheric conditions are listed in Table 1. Notably, the apparent kinetic parameters determined for the individual reactions in a stream of dry N_2 are practically identical with those obtained in our previous studies.[40, 53]

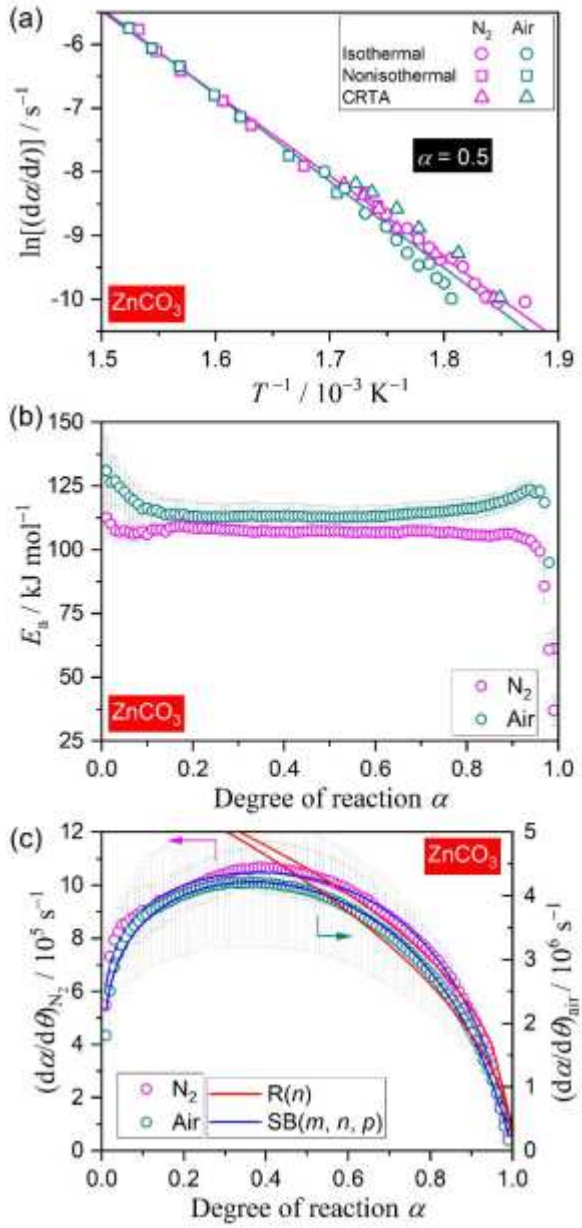

Figure 4. Formal kinetic analysis for the mass loss process of the thermal decomposition of $ZnCO_3$ in a stream of N_2 and air: (a) Friedman plots at $\alpha = 0.50$; (b) E_a values at different α values; (c) experimental master plots of $(d\alpha/dt)$ versus α and the fit curves using SB(m, n, p) ($0.01 \leq \alpha \leq 0.99$) and R($n$) ($0.40 \leq \alpha \leq 0.95$) models.

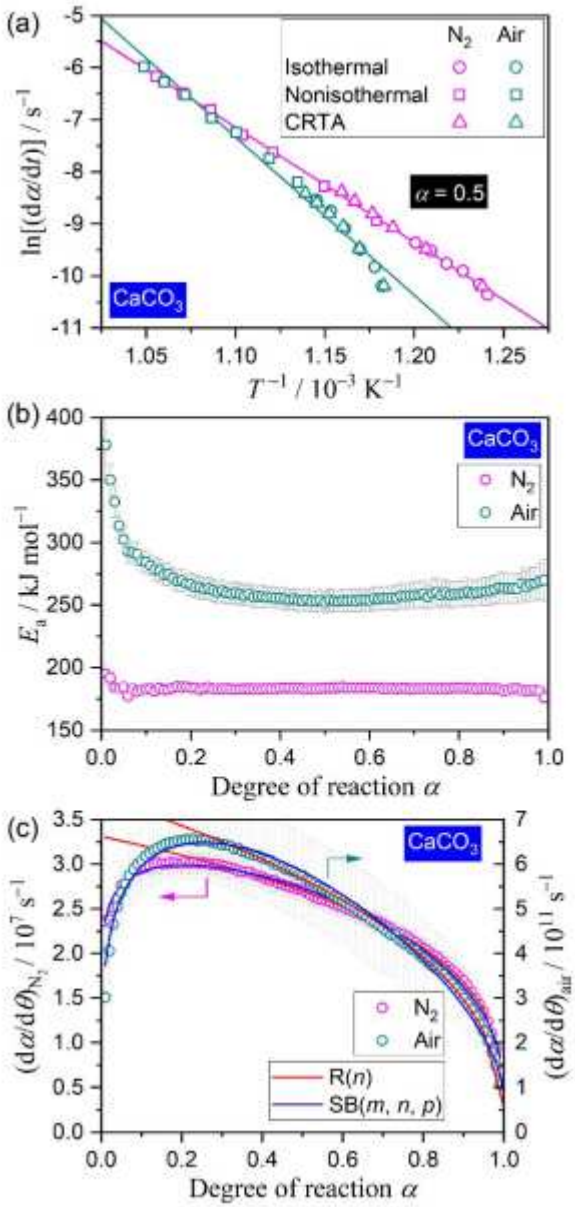

Figure 5. Formal kinetic analysis for the mass loss process of the thermal decomposition of $CaCO_3$ in a stream of N_2 and air: (a) Friedman plots at $\alpha = 0.50$; (b) E_a values at different α values; (c) experimental master plots of $(d\alpha/dt)$ versus α and the fit curves using SB(m, n, p) ($0.01 \leq \alpha \leq 0.99$) and R($n$) ($0.30 \leq \alpha \leq 0.95$) models.

Based on the analysis of the isoconversional kinetic relationship, the isothermal kinetic relationship was examined by drawing experimental master plots at an infinite temperature. The rate behavior extrapolated to an infinite temperature can be simulated by calculating the reaction rate ($d\alpha/d\theta$) at the infinite temperature and different α values: [74-79]

$$\frac{d\alpha}{d\theta} = \left(\frac{d\alpha}{dt}\right)\exp\left(\frac{E_a}{RT}\right) = Af(\alpha), \quad (7)$$

with $$\theta = \int_0^t \exp\left(-\frac{E_a}{RT}\right)dt,$$

where θ represents Ozawa's generalized time denoting the hypothetical reaction time at an infinite temperature. [80-81] In practice, $d\alpha/d\theta$ values at different α values were calculated using the average E_a value in the α range of 0.1–0.9 for each reaction and under different atmospheric conditions. For the thermal decomposition of $ZnCO_3$, the experimental master plots of $d\alpha/d\theta$ versus α for the reactions in a stream of dry N_2 and air had comparable shapes (Figure 4(c)), even though slightly larger $d\alpha/d\theta$ values were obtained in a stream of air. Each master plot was fitted using an empirical $f(\alpha)$ known as the Šesták-Berggren model (SB(m, n, p)). [82-84]

$$\mathrm{SB}(m,n,p): f(\alpha) = \alpha^m(1-\alpha)^n[-\ln(1-\alpha)]^p \quad (8)$$

Because of the superior flexibility of SB(m, n, p) to fit various types of isothermal rate behavior, both experimental master plots under different atmospheric conditions were perfectly fitted by optimizing the kinetic exponents (m, n, p) and A values (Figure 4(c) and Table 1). Although the kinetic exponents optimized for the thermal decomposition of $ZnCO_3$ in a stream of dry N_2 and air were practically comparable, the larger A value was obtained in a stream of air. Considering the reaction geometry of the thermal decomposition of solids, a contracting geometry model can be applied to the deceleration stage of the reaction. Thus, the deceleration part of the experimental master plots was also fitted using a phase boundary-controlled model (R(n)).[85]

$$\mathrm{R}(n): f(\alpha) = n(1-\alpha)^{1-1/n} \quad (9)$$

The deceleration part of the experimental master plots ($0.40 \le \alpha \le 0.95$) in a stream of dry N_2 and air was best fitted with $n = 1.75$ and 2.09, respectively, indicating two-dimensional interface shrinkage controlled by the chemical reaction. For the thermal decomposition of $CaCO_3$, the shapes of the experimental master plots in a stream of dry N_2 and air significantly differed (Figure 5(c)). The $d\alpha/d\theta$ values for the reaction in a stream of air were larger by four-order than those in a stream of dry N_2. The individual experimental master plots were perfectly fitted by SB(m, n, p), but the optimized kinetic exponents differed significantly between the reactions in a stream of dry N_2 and air (Table 1). Meanwhile, fittings of the deceleration part of the experimental master plots ($0.30 \le \alpha \le 0.95$) using the R(n) model provided n =1.42 and 1.67 for the reactions in a stream of dry N_2 and air.

Table 1. Results of formal kinetic analysis for the thermal decomposition of $ZnCO_3$ and $CaCO_3$ in a stream of dry N_2 and air

Sample	Atmosphere	E_a / kJ mol^{-1}, [a]	$(d\alpha/d\theta) = Af(\alpha)$					
			$f(\alpha)$	A / s^{-1}	m	n	p	R^2, [e]
$ZnCO_3$	N_2	107.2 ± 0.9	SB(m, n, p), [b]	(1.38 ± 0.02) × 10^6	−2.57 ± 0.15	1.54 ± 0.06	2.75 ± 0.15	0.9963
			R(n), [c]	(8.19 ± 0.07) × 10^5	-----	1.75 ± 0.03	-----	0.9777
	Air	114.2 ± 1.8	SB(m, n, p), [b]	(6.15 ± 0.11) × 10^6	−2.28 ± 0.15	1.54 ± 0.06	2.51 ± 0.14	0.9978
			R(n), [c]	(2.89 ± 0.04) × 10^6	-----	2.09 ± 0.05	-----	0.9818
$CaCO_3$	N_2	183.4 ± 0.6	SB(m, n, p), [b]	(3.90 ± 0.05) × 10^7	0.63 ± 0.10	0.16 ± 0.04	−0.52 ± 0.10	0.9943
			R(n), [d]	(2.33 ± 0.01) × 10^7	-----	1.42 ± 0.01	-----	0.9994
	Air	259.7 ± 6.9	SB(m, n, p), [b]	(1.09 ± 0.02) × 10^{12}	1.72 ± 0.15	−0.03 ± 0.06	−1.49 ± 0.14	0.9931
			R(n), [d]	(4.48 ± 0.01) × 10^{11}	-----	1.67 ± 0.01	-----	0.9992

[a] Averaged range: $0.10 \leq \alpha \leq 0.90$

[b] Fitted range: $0.01 \leq \alpha \leq 0.99$.

[c] Fitted range: $0.40 \leq \alpha \leq 0.95$.

[d] Fitted range: $0.30 \leq \alpha \leq 0.95$.

[e] Determination coefficient of the nonlinear least-squares analysis.

3.3 Effect of self-generated CO_2 on the overall kinetics

The results of the conventional kinetic analysis for the thermal decomposition processes of $ZnCO_3$ and $CaCO_3$ indicated the detectable effects of atmospheric CO_2 even in a stream of air with a limited $p(CO_2)$. Thus, the kinetic equation in eq. (1) considering the effect of $p(CO_2)_{ATM}$ in the AF (eq. (2)) should be used to describe the thermal decomposition in a stream of air.[40, 49-51, 53, 55] With an extended definition of (a, b) as independent variables, eq. (2) can be used as an analytical function to estimate the physico-chemical feature of the effect of $p(CO_2)$ using the optimized exponents (a, b). Furthermore, the contribution of the self-generated CO_2 should be considered to reveal the effect of $p(CO_2)$ on the kinetics of the thermal decomposition even in a stream of dry N_2 gas, as expected from the changes in the CO_2 concentration in the outflow gas during the thermal decomposition of $ZnCO_3$ and $CaCO_3$ (Figures 2, 3, S2, and S3). The CO_2 partial pressure attributed to the self-generated CO_2, i.e., $p(CO_2)_{SG}$, can be a certain value proportional to the evolution rate of CO_2. Thus, the $p(CO_2)$ value in eq. (2) is expressed using a weighted sum of $p(CO_2)_{SG}$ and a portion of the atmospheric $p(CO_2)_{ATM}$.[40]

$$p(\mathrm{CO_2}) = p(\mathrm{CO_2})_{\mathrm{SG}} + d \cdot p(\mathrm{CO_2})_{\mathrm{ATM}} = c \cdot \left(\frac{\mathrm{d}\alpha}{\mathrm{d}t}\right) + d \cdot p(\mathrm{CO_2})_{\mathrm{ATM}} \qquad (10)$$

where c represents the proportional constant in the relationship of $p(CO_2)_{SG}$ versus ($d\alpha/dt$), and d represents the contribution of $p(CO_2)_{ATM}$. Notably, the parameters (c, d) are the empirical values that change depending on the m_0 and q_v of atmospheric gas. By introducing the AF (eq. (2)) with $p(CO_2)$ in eq. (10), eq. (1) universally describes the kinetics of the thermal decomposition over different $p(CO_2)$ values considering both $p(CO_2)_{SG}$ and $p(CO_2)_{ATM}$. The isoconversional kinetic relationship for the thermal decomposition under different $p(CO_2)$ conditions is expressed using the logarithmic form of eq. (1):[40, 49-51, 53, 55]

$$\ln\frac{\left(\frac{\mathrm{d}\alpha}{\mathrm{d}t}\right)}{h(p(\mathrm{CO_2}),P_{\mathrm{eq}}(T))} = \ln[Af(\alpha)] - \frac{E_{\mathrm{a}}}{RT} \qquad (11)$$

Ideally, at a selected α value, all data points should be on a single straight line when plotting the lefthand side of eq. (11) versus the reciprocal temperature (i.e., the extended Friedman plot). To achieve an ideal single linear plot, the parameters in $h(p(CO_2), P_{eq}(T))$, i.e., (a, b, c, d), should be optimized during the extended Friedman plot at individual α values.

In our previous studies on the kinetics of the thermal decomposition of $ZnCO_3$ and $CaCO_3$ at various atmospheric $p(CO_2)$ values, [40, 53] the exponents (a, b) in eq. (2) were determined without considering the contributions of $p(CO_2)_{SG}$ (Table S2). The previously reported exponents (a, b) were used as the initial values for the extended Friedman plots considering the contributions of $p(CO_2)_{SG}$ in addition to $p(CO_2)_{ATM}$. Figures 6 and 7 show the results of the extended Friedman plots considering both $p(CO_2)_{SG}$ and $p(CO_2)_{ATM}$ for the thermal decompositions of $ZnCO_3$ and $CaCO_3$, respectively. Irrespective of the α value, the extended Friedman plots exhibited a single straight line that include all data points recorded in a stream of dry N_2 and air (Figures 6(a) and 7(a)) by optimizing the parameters (a, b, c, d). The optimized exponents at different α values exhibited approximately constant values during the respective reactions (Figures 6(b) and 7(b)). The E_a values calculated from the extended Friedman plots were also constant during the

majority of the reactions ($0.10 \leq \alpha \leq 0.90$ and $0.20 \leq \alpha \leq 0.80$ for the thermal decomposition of $ZnCO_3$ and $CaCO_3$, respectively) (Figures 6(c) and 7(c)). Averaged values of the parameters (*a*, *b*, *c*, *d*) in the AF and E_a values are listed in Table 2. E_a values were recalculated using the average parameters (*a, b*, *c*, *d*) in Table 2 for the extended Friedman plots at different α values, which improved the constancy of E_a values at different α values. The average E_a values recalculated using the average (*a*, *b*, *c*, *d*) values were 227.0 ± 0.8 kJ mol^{-1} ($0.10 \leq \alpha \leq 0.90$) and 1145 ± 6 kJ mol^{-1} ($0.20 \leq \alpha \leq 0.80$) for the thermal decomposition of $ZnCO_3$ and $CaCO_3$, respectively (Figures 6(c) and 7(c)). Notably, the E_a values determined by considering the effects of $p(CO_2)_{SG}$ and $p(CO_2)_{ATM}$ for the individual reactions in a stream of dry N_2 and air closely correspond to those determined for the reactions at greater $p(CO_2)_{ATM}$ values in our previous studies.[40, 53]

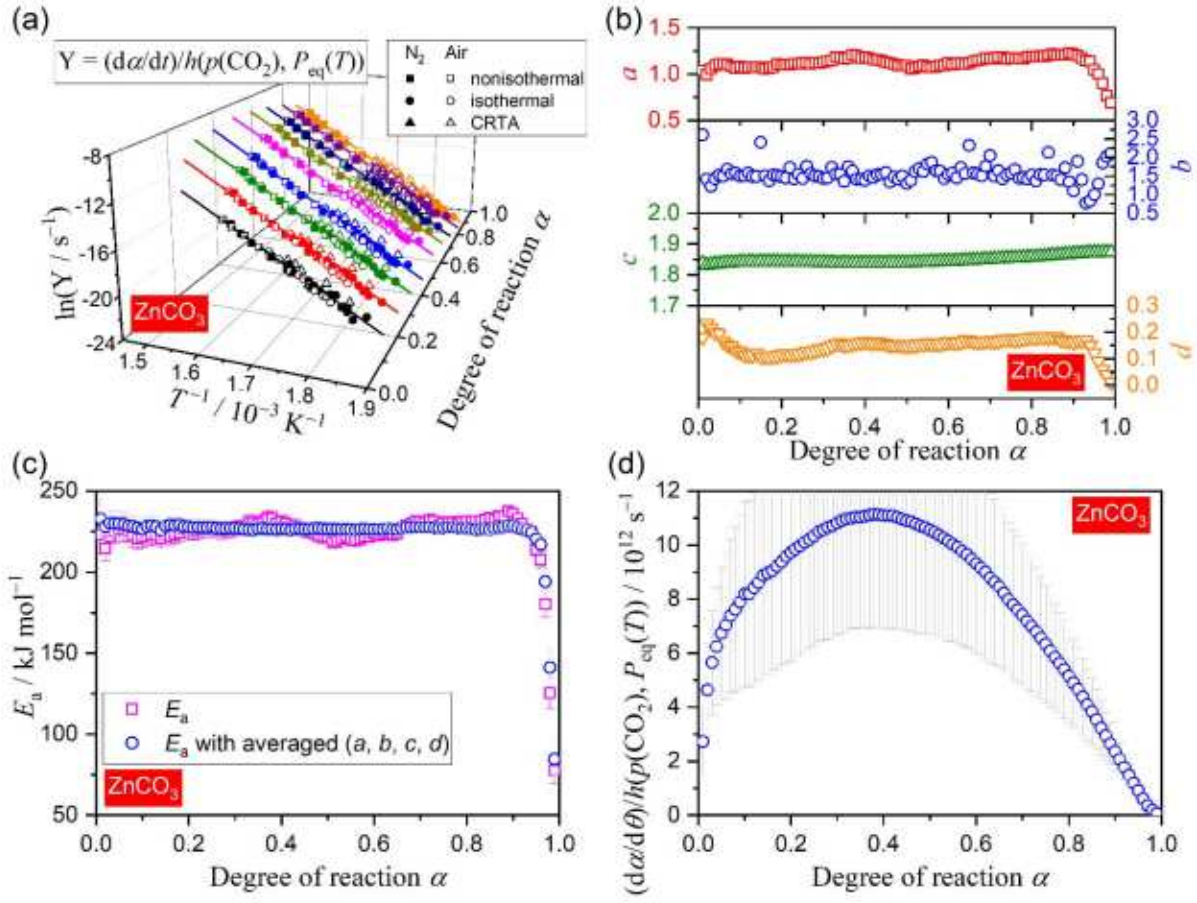

Figure 6. Results of the extended Friedman and master plot analyses for the thermal decomposition of $ZnCO_3$ in a stream of dry N_2 and air considering the effect of self-generated and atmospheric CO_2: (a) extended Friedman plots at different α values; (b) optimized parameters (*a*, *b*, *c*, *d*) in AF (eqs. (2) and (10)) at different α values; (c) E_a values at different α values; (d) extended experimental master plot of $(d\alpha/d\theta)/h(p(CO_2), P_{eq}(T))$ versus α.

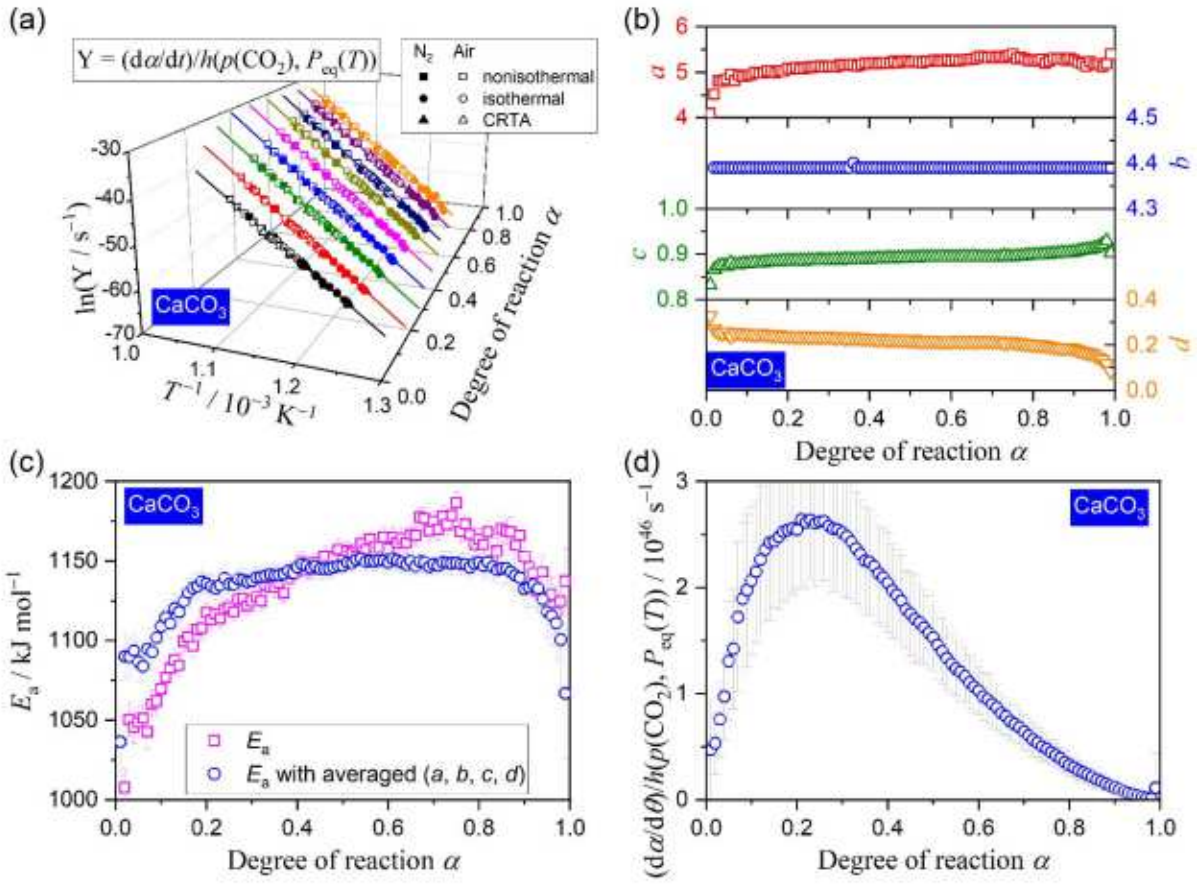

Figure 7. Results of the extended Friedman and master plot analyses for the thermal decomposition of $CaCO_3$ in a stream of dry N_2 and air considering the effect of self-generated and atmospheric CO_2: (a) extended Friedman plots at different α values; (b) optimized parameters (a, b, c, d) in AF (eqs. (2) and (10)) at different α values; (c) E_a values at different α values; (d) extended experimental master plot of $(d\alpha/d\theta)/h(p(CO_2), P_{eq}(T))$ versus α.

Table 2. The optimized parameters (*a*, *b*, *c*, *d*) in the AF (eqs. (2) and (10)) and E_a determined from extended Friedman plots of the thermal decomposition of $ZnCO_3$ and $CaCO_3$ in a stream of dry N_2 and air

Reactant	Condition	a [a]	b [a]	c [a]	d [a]	E_a / kJ mol^{-1} [b]
$ZnCO_3$	$a \neq b$	1.13 ± 0.05	1.56 ± 0.21	1.85 ± 0.01	0.15 ± 0.03	227.0 ± 4.5
	$a = b$	1.13 ± 0.05		1.85 ± 0.01	0.14 ± 0.02	227.0 ± 4.5
$CaCO_3$	$a \neq b$	5.20 ± 0.11	4.39 ± 0.01	0.89 ± 0.01	0.22 ± 0.02	1150 ± 19
	$a = b$	5.20 ± 0.11		0.89 ± 0.01	0.22 ± 0.02	1150 ± 19

[a] Averaged over $0.10 \leq \alpha \leq 0.90$.

[b] Averaged over $0.10 \leq \alpha \leq 0.90$ ($ZnCO_3$) or $0.20 \leq \alpha \leq 0.80$ ($CaCO_3$).

In the extended Friedman plot based on eq. (11) examined using the analytical form of AF (eq. (2)), the contribution of $(p(CO_2)/P_{eq}(T))^b$ was limited compared with $(1/p(CO_2))^a$ in both $ZnCO_3$ and $CaCO_3$. Therefore, the optimized exponent b can have an arbitrary value. Although the exponents (a, b) were set to be independent for analytical purposes in examining the extended Friedman plots presented in Figures 6 and 7, identical values of a and b have been theoretically justified while deriving the AF based on the multistep chemical process of interfacial reaction,[40, 49-59] The identical values of a and b in the AF is derived for the interfacial process controlled by an elementary step of the consumption of interstitial CO_2 defects and formation of the solid product building unit, where a (= b) value denotes the coefficient of the defect in the chemical equation of the elementary step. Reexamination of the extended Friedman plots with the restriction of $a = b$ provided comparable results with the previous examination by assuming independent a and b values, as depicted in Figures S8 and S9 for the thermal decomposition of $ZnCO_3$ and $CaCO_3$, respectively. Only the b value changed to be identical to the previously determined a value by assuming independent a and b values in both reactions, whereas the exponent a and the apparent E_a values were practically unchanged, as listed in Table 2. Under this calculation condition, the extended Friedman plot simultaneously examines the temperature dependences of $(d\alpha/dt)$ based on the Arrhenius relationship (eq. (3)) and that of a-th (= b-th)-powered $P_{eq}(T)$ based on the van't Hoff plot:

$$a\ln P_{eq}(T) = -\frac{a\Delta_r H^\circ}{RT} + \frac{a\Delta_r S^\circ}{R}, \qquad (12)$$

where $\Delta_r H^\circ$ and $\Delta_r S^\circ$ denote the standard enthalpy and entropy of the reaction, respectively. Subtracting eq. (12) from eq. (11) with the AF (eq. (2), $a = b$), we obtain the following equation:

$$\ln\left[\left(\frac{d\alpha}{dt}\right)\frac{p(CO_2)^a}{P_{eq}(T)^a - p(CO_2)^a}\right] = -\frac{E_a - a\Delta_r H^\circ}{RT} + \ln\left[Af(\alpha)\exp\left(-\frac{a\Delta_r S^\circ}{R}\right)\right]. \qquad (13)$$

When $p(CO_2)^a/(P_{eq}(T)^a - p(CO_2)^a)$ can be approximated to be a constant value, the intrinsic E_a value ($E_{a,int.}$) based on the Arrhenius relationship is expressed as follows. [40, 52, 86-89]

$$E_{a,int} \approx E_a - a\Delta_r H^\circ \qquad (14)$$

Based on eq. (14), the $E_{a,int}$ values are roughly estimated to be 152 and 259 kJ mol^{-1} for the thermal decomposition of $ZnCO_3$ and $CaCO_3$, respectively, using the experimentally determined exponent a and apparent E_a values listed in Table 2 and the $\Delta_r H^\circ$ value calculated using thermodynamic software (MALT2, Kagaku Gijutsu-Sha[90-91]): $\Delta_r H^\circ_{625\ K} = 66.7$ kJ mol^{-1} for $ZnCO_3$ and $\Delta_r H^\circ_{900\ K} = 171.4$ kJ mol^{-1} for $CaCO_3$. These $E_{a,\ int}$ values are significantly larger than those determined without considering the effect of self-generated CO_2 for the reactions in a stream of dry N_2 gas for both reactions of $ZnCO_3$ and $CaCO_3$ (Table 1), but are expected to be invariant for the reactions at different temperatures and $p(CO_2)$ values.

By introducing the AF into eq. (7), the experimental master plot universally describing the isothermal kinetic relationship under different temperature and $p(CO_2)$ conditions can be formulated according to eq. (15). [40, 53, 57]

$$\frac{\left(\frac{\mathrm{d}\alpha}{\mathrm{d}\theta}\right)}{h(p(\mathrm{CO_2}),P_{\mathrm{eq}}(T))} = \frac{\left(\frac{\mathrm{d}\alpha}{\mathrm{d}t}\right)\exp\left(\frac{E_\mathrm{a}}{RT}\right)}{h(p(\mathrm{CO_2}),P_{\mathrm{eq}}(T))} = Af(\alpha) \qquad (15)$$

The values of the left-hand side of eq. (15) were calculated using the AF of eqs. (2) and (10) with average values of (a, b, c, d) (Table 2) and E_a at different α values. For both reactions, the extended experimental master plots of $(\mathrm{d}\alpha/\mathrm{d}\theta)/h(p(\mathrm{CO_2}), P_{\mathrm{eq}}(T))$ versus α exhibited a maximum reaction rate midway through the reaction (at α = 0.39 and 0.21 for the thermal decomposition of $ZnCO_3$ and $CaCO_3$, respectively; Figures 6(d) and 7(d)). The shapes of the extended experimental master plots are significantly different from the conventional experimental master plots drawn without considering the effect of $p(CO_2)$ (Figures 4(c) and 5(c)), with the acceleration and deceleration stages being more distinguished. Notably, practically the same rate behavior was estimated from the examination of the experimental master plot by assuming $a = b$ in the AF (eq. (2)), as depicted in Figures S8(d) and S9(d) for the reactions of $ZnCO_3$ and $CaCO_3$, respectively. Such rate behavior observed for the thermal decomposition of inorganic solids constrained by the contracting geometry reaction scheme can be described by the physico-geometrical consecutive process comprising the SR and PBR as formulated by the Mampel-type models.[65, 92-93]

3.4 Effect of self-generated CO_2 on physico-geometrical consecutive reaction steps

The kinetic analysis based on the SR–PBR model originated from Mampel's model.[93] Ogasawara and Koga derived the differential kinetic equations under isothermal conditions by assuming the first-order process for the SR and different shrinkage dimensions for the PBR process (Table S3).[65] The results of the kinetic analysis based on SR–PBR(n) models for the thermal decomposition of $ZnCO_3$ and $CaCO_3$ under isothermal conditions in a stream of dry N_2 and air are depicted in Figures 8 and S10 for $ZnCO_3$ and Figures 9 and S11 for $CaCO_3$. The different SR–PBR(n) models were fitted to each experimental kinetic curve by optimizing the rate constants for the SR and PBR(n) processes, i.e., k_{SR} and $k_{\mathrm{PBR}(n)}$. For both reactions, irrespective of atmospheric conditions, statistically significant fits to experimental kinetic curves were achieved using the SR–PBR(2) (Figures 8(a), (b) and 9(a), (b)) and SR–PBR(3) (Figures S10(a), (b) and S11(a), (b)) models. Given the residual sum of square and determination coefficient (R_2), using the SR–PBR(2) model resulted in slightly better fitting in both reactions (Tables S4 and S5).

Tentatively, the individual temperature dependences of optimized k_{SR} and $k_{\mathrm{PBR}(n)}$ values were examined using the conventional Arrhenius plot.

$$\ln k = \ln A - \frac{E_\mathrm{a}}{RT} \qquad (16)$$

The conventional Arrhenius plots for k_{SR} and $k_{\mathrm{PBR}(n)}$ exhibited different linear correlations for the processes in a stream of dry N_2 and air (Figures 8(c), (d) and S10(c), (d) for $ZnCO_3$ and Figures 9(c), (d) and S11(c), (d) for $CaCO_3$). Irrespective of the physico-geometrical process, a larger difference in the slope of the Arrhenius plots for the reactions in a stream of dry N_2 and air was observed for the thermal decomposition of $CaCO_3$. The apparent Arrhenius parameters for the SR and PBR(n) processes determined by the conventional Arrhenius plot are summarized in Table S6. The apparent values of Arrhenius parameters were larger in a stream of air than in a stream of dry N_2 in both SR and PBR(n) processes. Although this trend was observed in both reactions of $ZnCO_3$ and $CaCO_3$, the thermal decomposition of $CaCO_3$

exhibited the larger increase in the apparent values of Arrhenius parameters by the change in the atmospheric conditions from dry N_2 to air. Comparing the apparent Arrhenius parameters for the SR and PBR(n) processes, opposite magnitude relationships were observed for the thermal decomposition of $ZnCO_3$ and $CaCO_3$: $(E_a, \ln A)_{SR} > (E_a, \ln A)_{PBR(n)}$ for $ZnCO_3$ and $(E_a, \ln A)_{SR} < (E_a, \ln A)_{PBR(n)}$ for $CaCO_3$.

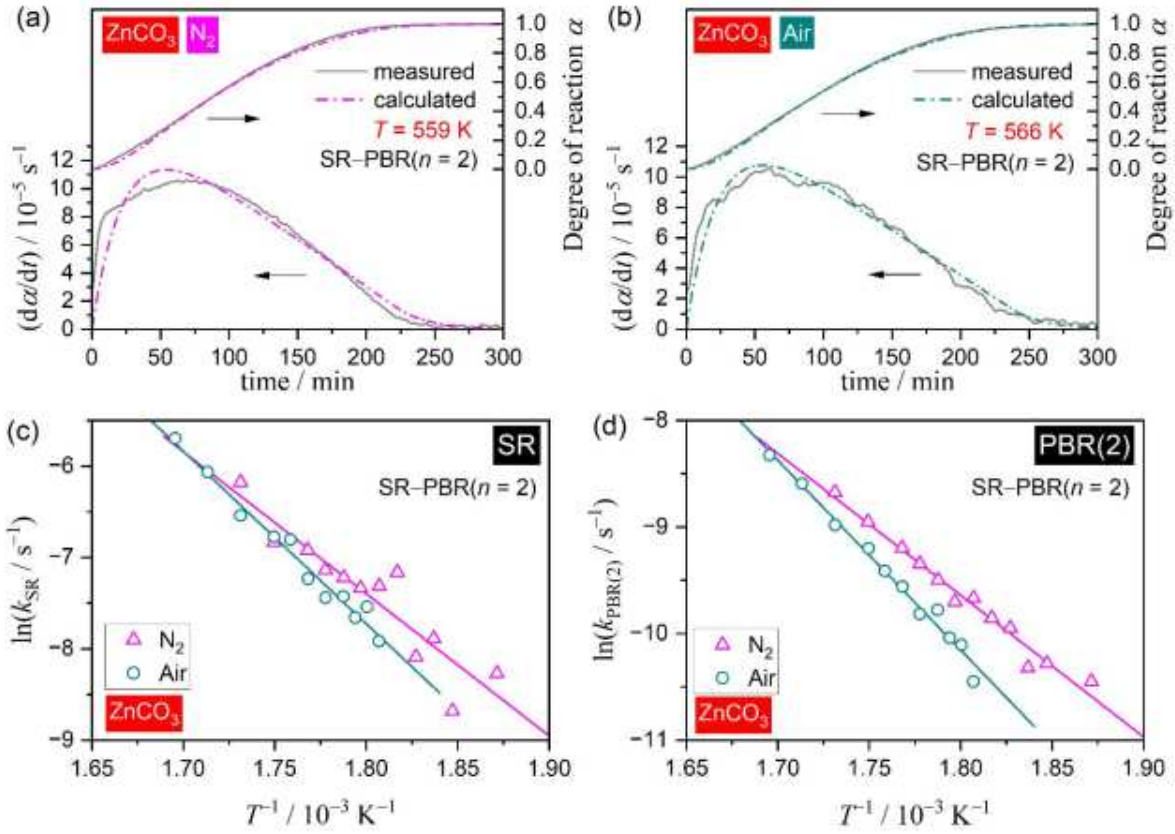

Figure 8. Kinetic analyses using the SR–PBR(2) model for the thermal decomposition of $ZnCO_3$ under isothermal conditions in a stream of dry N_2 and air: (a) typical fitting to the isothermal kinetic curve (T = 559 K) in a stream of dry N_2; (b) typical fitting to the isothermal kinetic curve (T = 566 K) in a stream of air; (c) conventional Arrhenius plots for SR; (d) conventional Arrhenius plots for PBR(2).

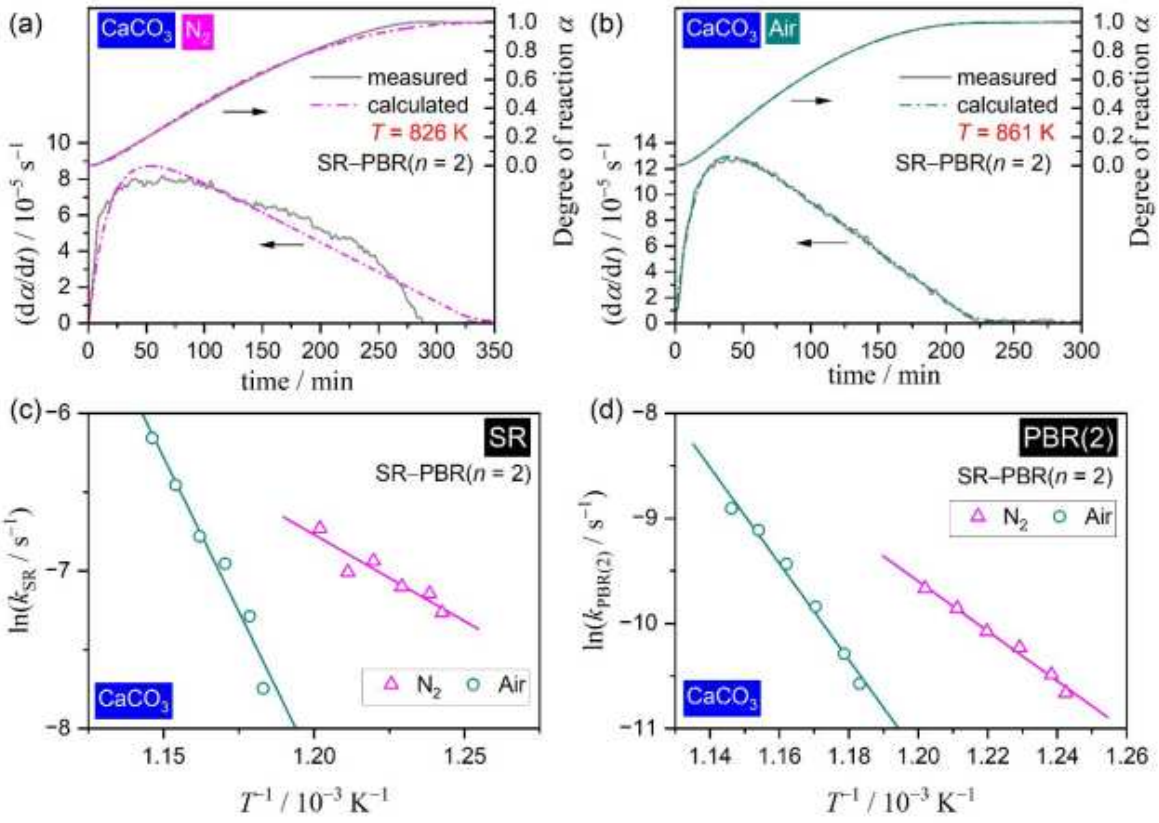

Figure 9. Kinetic analyses using the SR–PBR(2) model for the thermal decomposition of $CaCO_3$ under isothermal conditions in a stream of dry N_2 and air: (a) typical fitting to the isothermal kinetic curve (T = 826 K) in a stream of dry N_2; (b) typical fitting to the isothermal kinetic curve (T = 861 K) in a stream of air; (c) conventional Arrhenius plots for SR; (d) conventional Arrhenius plots for PBR(2).

To realize a universal kinetic description for each physico-geometrical reaction step in a stream of dry N_2 and air, the AF in eq. (2) is introduced into the basic Arrhenius equation.[40, 49-51, 53, 55-57]

$$\ln\frac{k}{\left(\frac{1}{p(\mathrm{CO_2})}\right)^{a}\left[1-\left(\frac{p(\mathrm{CO_2})}{P_{\mathrm{eq}}(T)}\right)^{b}\right]} = \ln A - \frac{E_a}{RT} \qquad (17)$$

In addition, the effective $p(CO_2)$ value was assumed to be the sum of the contributions of $p(CO_2)_{SG}$ and $p(CO_2)_{ATM}$. Furthermore, the $p(CO_2)_{SG}$ value was set to be proportional to the k value with the proportionality constant (c). [40]

$$p(\mathrm{CO_2}) = p(\mathrm{CO_2})_{\mathrm{SG}} + d \cdot p(\mathrm{CO_2})_{\mathrm{ATM}} = c \cdot k + d \cdot p(\mathrm{CO_2})_{\mathrm{ATM}}, \qquad (18)$$

Initially, the exponents (a, b) in eq. (2) determined through the extended Friedman plot were introduced into eq. (17), and the parameters (c, d) in eq. (18) were optimized to produce the best linearity of the extended Arrhenius plot (eq. (17)) including all k_{SR} or $k_{PBR(n)}$ values in a stream of dry N_2 and air. After that, using the parameters (a, b, c, d) as the initial values, all parameters were further optimized to produce the best linear correlation. Figures 10 and 11

show the extended Arrhenius plots of the individual physico-geometrical reaction steps of the SR–PBR(2) model for the thermal decomposition of $ZnCO_3$ and $CaCO_3$, respectively. The counterpart results based on the SR–PBR(3) model are shown in Figures S12 and S13, respectively. In each physico-geometrical reaction step, all k values determined at different temperatures in a stream of dry N_2 and air generated a single straight line with a statistically significant linear correlation after optimizing a–d values.

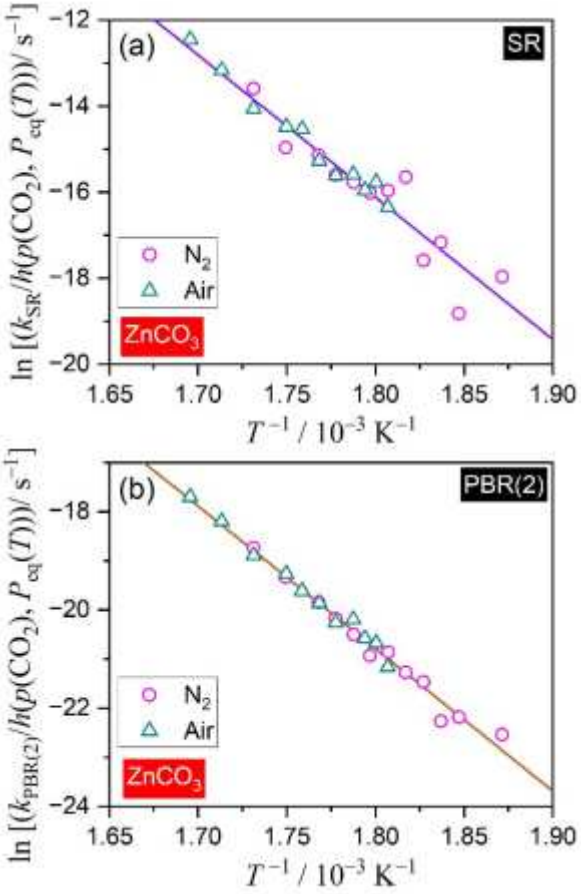

Figure 10. Extended Arrhenius plots for individual physico-geometrical reaction steps (SR–PBR(2)) of the thermal decomposition of $ZnCO_3$ under isothermal conditions in a stream of dry N_2 and air: (a) SR and (b) PBR(2) processes.

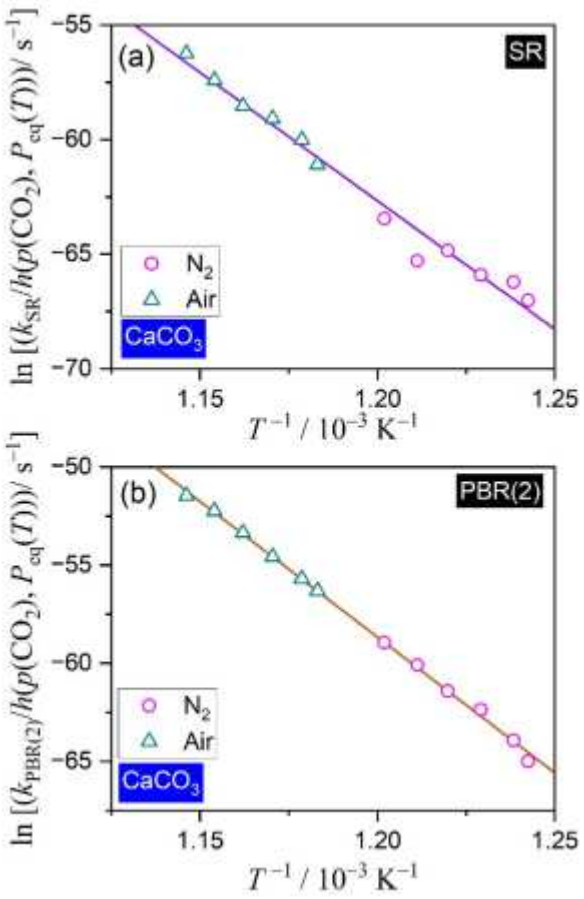

Figure 11. Extended Arrhenius plots for individual physico-geometrical reaction steps (SR–PBR(2)) of the thermal decomposition of $CaCO_3$ under isothermal conditions in a stream of dry N_2 and air: (a) SR and (b) PBR(2) processes.

Table 3 lists the kinetic parameters including the Arrhenius parameters and exponents *a–d* in the AF (eqs. (2) and (18)) determined for the individual physico-geometrical reaction steps of the thermal decomposition of $ZnCO_3$ and $CaCO_3$ in a stream of dry N_2 and air. In both reactions, the kinetic parameters determined based on SR–PBR(2) and SR–PBR(3) were comparable in each physico-geometrical reaction step. The Arrhenius parameters, E_a and ln*A*, determined by the extended Arrhenius plots increased and decreased as the reaction step progressed from SR to PBR for the thermal decomposition of $ZnCO_3$ and $CaCO_3$, respectively. The smaller E_a value for the SR than PBR observed for $CaCO_3$ seems to have originated from the specific characteristics of the $CaCO_3$ sample used in this study, which has a small particle size (Figure S1(b), 0.4 ± 0.3 μm) and a large specific surface area (S_{BET} = 6.6 ± 0.1 $m^2\ g^{-1}$).[39] The higher reactivity of the $CaCO_3$ sample surface in comparison with the other calcite samples with larger particle sizes has been confirmed in view of reaction initiation temperature in our previous study.[39] The E_a value for the PBR process agreed with that determined by the extended Friedman plot in both reactions (Table 2). The exponents *a* and *b* in the AF were also comparable with those determined through the extended Friedman plot. These *a* and *b* values were also coincident with those determined for the reactions in a higher $p(CO_2)$ value range in our previous studies.[40, 53] Therefore, the AF in eq. (2) with these exponents *a* and *b* can be

universally applied to the respective thermal decomposition of $ZnCO_3$ and $CaCO_3$ over a range of $p(CO_2)$ from self-generated $p(CO_2)$ to atmospheric $p(CO_2)$ of up to 20 kPa. When considering the effective $p(CO_2)$ as a weighted sum of the $p(CO_2)_{SG}$ and $p(CO_2)_{ATM}$, the contribution of the $p(CO_2)_{SG}$ was parameterized as the parameter c, as in the case of the extended Friedman plot (Figures 6 and 7). In both reactions, the parameter c increased as the physico-geometrical reaction step advanced from the SR to PBR. During the SR process, the self-generated CO_2 is immediately removed from the reaction site, restricting its contribution. However, in the PBR process, CO_2 produced at the internal reaction interface is removed by diffusion through the surface product layer. Accordingly, the larger contribution of the $p(CO_2)_{SG}$ to the effective $p(CO_2)$ is expected for the PBR process. The expected trend of the change in the contribution of the $p(CO_2)_{SG}$ to the kinetics is more evident for the thermal decomposition of $CaCO_3$, where the parameter c is negligible for the SR process and approaches unity for the PBR process. The parameter c for the PBR process is also coincident with that determined through the extended Friedman plot ($c = 0.89 \pm 0.01$).

Table 3. Kinetic parameters including the Arrhenius parameters and exponents a–d in the AF, determined through the extended Arrhenius plots for individual reaction steps of the thermal decomposition of $ZnCO_3$ and $CaCO_3$ in a stream of dry N_2 and air

Sample	Model	Condition	Step	a	b	c	d	E_a/kJ mol^{-1}	$\ln[(A/h(p(CO_2), P_{eq}(T))/s^{-1}]$	$-\gamma$ [a]
$ZnCO_3$	SR–PBR(2)	$a \neq b$	SR	1.09	1.56	0.52	0.48	275 ± 18	43.4 ± 3.9	0.9590
			PBR(2)	1.15	1.56	0.90	0.12	241 ± 7	31.4 ± 1.4	0.9929
		$a = b$	SR	1.09		0.52	0.48	275 ± 18	43.5 ± 3.9	0.9590
			PBR(2)	1.15		0.90	0.12	241 ± 7	31.4 ± 1.4	0.9929
	SR–PBR(3)	$a \neq b$	SR	1.10	1.56	0.62	0.38	271 ± 15	42.0 ± 3.1	0.9719
			PBR(3)	1.15	1.56	0.90	0.10	238 ± 8	30.2 ± 1.8	0.9883
		$a = b$	SR	1.10		0.62	0.38	271 ± 15	42.1 ± 3.1	0.9719
			PBR(3)	1.15		0.90	0.10	237 ± 8	30.1 ± 1.8	0.9883
$CaCO_3$	SR–PBR(2)	$a \neq b$	SR	5.67	4.39	0.04	0.13	931 ± 44	71.8 ± 6.3	0.9893
			PBR(2)	5.09	4.39	0.98	0.20	1150 ± 15	107.3 ± 2.2	0.9991
		$a = b$	SR	5.67		0.04	0.13	921 ± 43	70.2 ± 6.2	0.9893
			PBR(2)	5.09		0.98	0.20	1152 ± 15	107.6 ± 2.2	0.9991
	SR–PBR(3)	$a \neq b$	SR	5.57	4.39	0.01	0.02	928 ± 73	62.7 ± 10.5	0.9704
			PBR(3)	4.99	4.39	1.07	0.18	1161 ± 24	108.7 ± 3.4	0.9979
		$a = b$	SR	5.57		0.01	0.02	920 ± 73	61.6 ± 10.4	0.9704
			PBR(3)	4.99		1.06	0.18	1166 ± 24	109.4 ± 3.4	0.9980

[a] Correlation coefficient of the linear regression analysis for the extended Arrhenius plot.

Notably, the results of the extended Arrhenius plot did not vary when the restriction of $a = b$ in the AF was introduced for optimizing a–d in both reactions, except for the change in the b value to be equal to the a value, as in the case of the Friedman plot (Figures S14–S17, Table 3). For the PBR(n) processes, the same discussion concerning the $E_{a,int}$ value based on eqs. (13) and (14) was possible in both reactions, obtaining an $E_{a,int}$ value comparable to that determined by the extended Friedman plot for individual reactions, e.g., 164 and 280 kJ mol^{-1} based on PBR(2) for $ZnCO_3$ and $CaCO_3$, respectively. For the SR process, however, a more realistic $E_{a,int}$ value was obtained from the results of the extended Arrhenius plot without the restriction of a

= b and using the optimized b value instead of the a value in eqs. (13) and (14). For the SR process of $ZnCO_3$, an $E_{a,int}$ value of 171 kJ mol^{-1} was obtained, which is slightly greater than that for PBR(2). In the case of the SR process of $CaCO_3$, we obtain a negative $E_{a,int}$ value from the results of the extended Arrhenius plot with the restriction of $a = b$. Besides, the results of the extended Arrhenius plot without the restriction of $a = b$ yielded an $E_{a,int}$ value of 179 kJ mol^{-1} using the optimized b value as the coefficient of the van't Hoff relationship (eq. (12)) instead of the a value. The $E_{a,int}$ value is significantly smaller than that for PBR(2), but it closely corresponds to the E_a value determined using the conventional kinetic equation (eq. (3)) for the reaction in a stream of dry N_2. Although the discussion concerning the $E_{a,int}$ value may be useful for correlating the kinetic analysis considering the effect of $p(CO_2)$ to the conventional one under a defined condition of the negligible effect of $p(CO_2)$, the refinement of the rough estimation of $E_{a,int}$ using eq. (14) should be a necessary future task crucial for obtaining universal kinetic descriptions at different temperatures and partial pressures of evolved gases for various reversible thermal decomposition reactions, along with the theoretical justification of the empirical kinetic procedure with strict consideration of the physical meaning of the AF and its exponents.

4. Conclusions

The kinetics of the thermal decomposition of $ZnCO_3$ and $CaCO_3$ in a stream of dry N_2 and air was reinvestigated to empirically parametrize the effect of self-generated gas on the kinetics of the reversible thermal decomposition of inorganic solids. Comparing the kinetic behavior of the thermal decomposition in a stream of dry N_2 and air, a retardation effect of CO_2 in the reaction atmosphere was evidenced in both $ZnCO_3$ and $CaCO_3$, with a more significant retardation effect observed for $CaCO_3$, as was expected from previous studies on the effect of atmospheric CO_2 in a range of atmospheric $p(CO_2)$ values greater than 1 kPa. In both reactions, the kinetic characteristics of the thermal decomposition in a stream of dry N_2 were approximately described by conventional kinetic analysis without considering the effect of CO_2 in the reaction atmosphere. However, the presence of CO_2 ($\approx$ 500 ppm) in the reaction atmosphere, which is expected to be smaller or comparable to the increase in the CO_2 concentration caused by the evolution as the gaseous product of the reaction, made applying conventional kinetic analysis difficult. In addition, the kinetic characteristics systematically varied with varying sample mass and flow rate of purge gas even in a stream of dry N_2. These observations indicate the necessity of an advanced kinetic approach considering the effect of both atmospheric and self-generated CO_2. In this study, an empirical procedure for parameterizing the effect of unmeasurable $p(CO_2)_{SG}$ on the kinetics of the thermal decomposition of $ZnCO_3$ and $CaCO_3$ was examined by considering the effective $p(CO_2)$ value during the reaction as a weighted sum of the contributions of $p(CO_2)_{SG}$ and $p(CO_2)_{ATM}$ (eq. (10)). Within the framework of the universal kinetic description at different temperatures and $p(CO_2)$ values formalized by introducing an analytical form of AF (eq. (2)) into the general kinetic equation (eq.(1)), the established kinetic relationships in the relatively higher $p(CO_2)_{ATM}$ values ($\geq$ 1 kPa) were extrapolated to the smaller $p(CO_2)_{ATM}$, i.e., in a stream of dry N_2 and air. Thereafter, the individual contributions of $p(CO_2)_{SG}$ and $p(CO_2)_{ATM}$ to the effective $p(CO_2)$ value were optimized to obtain the best linear kinetic relationship with regard to the extended Arrhenius-type plots. The thermal decomposition processes of $ZnCO_3$ and $CaCO_3$ in a stream of dry N_2 and air could be universally described by optimizing the exponents (a, b) in the AF (eq. (2)) and the contributions (c, d) of

$p(CO_2)_{SG}$ and $p(CO_2)_{ATM}$ (eq. (10)), respectively. The apparent E_a values determined using the extended Friedman plots with the optimized parameters (a, b, c, d) were approximately constant during individual reactions: 227 and 1150 kJ mol^{-1} for $ZnCO_3$ and $CaCO_3$, respectively. Through the isoconversional kinetic approach, the parameter c that empirically expresses the contribution of $p(CO_2)_{SG}$ was optimized to be 1.85 and 0.89 for the reactions of $ZnCO_3$ and $CaCO_3$, respectively, indicating the actual contributions of the self-generated CO_2 to the kinetics. Considering the contribution of the temperature dependence of $P_{eq}(T)$ to the extended Friedman plot, the E_a values intrinsic in the Arrhenius relationship were roughly estimated to be 152 and 259 kJ mol^{-1} for the thermal decomposition of $ZnCO_3$ and $CaCO_3$, respectively.

Furthermore, the extended experimental master plots considering the effect of $p(CO_2)$ exhibited different shapes from those drawn without considering the effect in both reactions. These extended experimental master plots were characterized by the maximum reaction rate midway through the reaction, indicating the consecutive SR and PBR processes as a suitable physicogeometrical reaction model. The isothermal kinetic curves were well-fitted by the SR–PBR(2) or SR– PBR(3) model in both reactions by optimizing the k_{SR} and k_{PBR} values at individual temperatures. The temperature and $p(CO_2)$ dependence of k_{SR} and k_{PBR} values were simultaneously evaluated using the extended Arrhenius plot by optimizing (a, b, c, d) values. The respective linear kinetic relationships of the extended Arrhenius plots were established for the SR and PBR processes, where the apparent E_a value for the PBR process agreed with that determined by the extended Friedman plot. The universal kinetic description for the SR–PBR process indicated the increase in the contribution of the self-generated CO_2 to the kinetics as the reaction progressed from the SR to PBR(2) considering the variation in the parameter c, i.e., from 0.52 to 0.90 for $ZnCO_3$ and from 0.04 to 0.98 for $CaCO_3$. The proposed kinetic analysis approach to the reversible thermal decomposition of solids based on kinetic descriptions at different temperatures and partial pressures of evolved gas can serve as a method for empirically estimating the effect of self-generated gas and gaining further kinetic insight into physico-chemical features. This kinetic analysis approach considering both effects of selfgenerated and atmospheric gases enables the universal description of the kinetic characteristics of reversible thermal decomposition of solids with a fixed series of kinetic parameters including the parameters (a, b, c, d), by avoiding unwanted variations in kinetic parameters with a small change in the reaction conditions caused by the variation in the effect of self-generated gas.

ASSOCIATED CONTENT

Supporting Information

The Supporting Information is available free of charge on the ACS Publications website at DOI: ????????.

S1. Formulation of accommodation function (Table S1); S2. Characteristics of the samples (Figure S1); S3. Thermal behavior (Figures S2 and S3); S4. Formal kinetic analysis (Figure S4–S7); S5.

Effect of self-generated CO_2 on the overall kinetics (Table S2; Figures S8 and S9); and S6. Effect of self-generated CO_2 on physico-geometrical consecutive reaction steps (Tables S3–S6; Figures S10–S17).

AUTHOR INFORMATION

Corresponding Author
*Tel./fax: +81-82-424-7092. E-mail: nkoga@hiroshima-u.ac.jp

Notes
The authors declare no competing financial interest.

ACKNOWLEDGEMENTS

The present work was supported by JSPS KAKENHI Grant Numbers 19K02708, 22H01011, and 22K02946.

References

1. Prigiobbe, V.; Polettini, A.; Baciocchi, R., Gas–Solid Carbonation Kinetics of Air Pollution Control Residues for CO2 Storage. *Chem. Eng. J.* **2009**, *148*, 270-278.
2. Perejón, A.; Romeo, L. M.; Lara, Y.; Lisbona, P.; Martínez, A.; Valverde, J. M., The CalciumLooping Technology for CO2 Capture: On the Important Roles of Energy Integration and Sorbent Behavior. *Appl. Energy* **2016**, *162*, 787-807.
3. Han, R.; Wang, Y.; Xing, S.; Pang, C.; Hao, Y.; Song, C.; Liu, Q., Progress in Reducing Calcination Reaction Temperature of Calcium-Looping CO2 Capture Technology: A Critical Review. *Chem. Eng. J.* **2022**, *450*, 137952.
4. Raganati, F.; Ammendola, P., Review of Carbonate-Based Systems for Thermochemical Energy Storage for Concentrating Solar Power Applications: State-of-the-Art and Outlook. *Energy Fuels* **2023**, *37*, 1777-1808.
5. Duran-Olivencia, F. J.; Gannoun, R.; Perez, A. T.; Valverde, J. M., Efficacy of Nanosilica Coatings in Calcium Looping Reactors. *Ind. Eng. Chem. Res.* **2023**, *62*, 1373-1389.
6. Yu, X.; Tang, Z.; Sun, D.; Ouyang, L.; Zhu, M., Recent Advances and Remaining Challenges of Nanostructured Materials for Hydrogen Storage Applications. *Prog. Mater. Sci.* **2017**, *88*, 1-48.
7. Sun, Y.; Shen, C.; Lai, Q.; Liu, W.; Wang, D.-W.; Aguey-Zinsou, K.-F., Tailoring Magnesium Based Materials for Hydrogen Storage through Synthesis: Current State of the Art. *Energy Storage Mater.* **2018**, *10*, 168-198.
8. Ouyang, L.; Chen, K.; Jiang, J.; Yang, X.-S.; Zhu, M., Hydrogen Storage in Light-Metal Based Systems: A Review. *J. Alloys Compd.* **2020**, *829*, 154597.
9. Huang, Y.; Cheng, Y.; Zhang, J., A Review of High Density Solid Hydrogen Storage Materials by Pyrolysis for Promising Mobile Applications. *Ind. Eng. Chem. Res.* **2021**, *60*, 2737-2771.
10. Usman, M. R., Hydrogen Storage Methods: Review and Current Status. *Renewable Sustainable Energy Rev.* **2022**, *167*, 112743.
11. Wu, Y.; Blamey, J.; Anthony, E. J.; Fennell, P. S., Morphological Changes of Limestone Sorbent Particles During Carbonation/Calcination Looping Cycles in a Thermogravimetric Analyzer (TGA) and Reactivation with Steam. *Energy Fuels* **2010**, *24*, 2768-2776.
12. Wang, C.; Zhou, X.; Jia, L.; Tan, Y., Sintering of Limestone in Calcination/Carbonation Cycles. *Ind. Eng. Chem. Res.* **2014**, *53*, 16235-16244.
13. Valverde, J. M.; Sanchez-Jimenez, P. E.; Perez-Maqueda, L. A., Relevant Influence of Limestone Crystallinity on CO2 Capture in the Ca-Looping Technology at Realistic Calcination Conditions. *Environ. Sci. Technol.* **2014**, *48*, 9882-9.
14. Valverde, J. M.; Sanchez-Jimenez, P. E.; Perez-Maqueda, L. A., High and Stable CO2 Capture Capacity of Natural Limestone at Ca-Looping Conditions by Heat Pretreatment and Recarbonation Synergy. *Fuel* **2014**, *123*, 79-85.
15. Sanchez-Jimenez, P. E.; Valverde, J. M.; Perez-Maqueda, L. A., Multicyclic Conversion of Limestone at Ca-Looping Conditions: The Role of Solid-Sate Diffusion Controlled Carbonation. *Fuel* **2014**, *127*, 131-140.
16. Valverde, J. M.; Sanchez-Jimenez, P. E.; Perez-Maqueda, L. A., Effect of Heat Pretreatment/Recarbonation in the Ca-Looping Process at Realistic Calcination Conditions. *Energy Fuels* **2014**, *28*, 4062-4067.

17. Valverde, J. M.; Sanchez-Jimenez, P. E.; Perejon, A.; Perez-Maqueda, L. A., CO2 Multicyclic Capture of Pretreated/Doped CaO in the Ca-Looping Process. Theory and Experiments. *Phys. Chem. Chem. Phys.* **2013**, *15*, 11775-93.
18. Nikulshina, V.; Gálvez, M. E.; Steinfeld, A., Kinetic Analysis of the Carbonation Reactions for the Capture of CO2 from Air Via the Ca(OH)2–CaCO3–CaO Solar Thermochemical Cycle. *Chem. Eng. J.* **2007**, *129*, 75-83.
19. Martínez, I.; Grasa, G.; Murillo, R.; Arias, B.; Abanades, J. C., Kinetics of Calcination of Partially Carbonated Particles in a Ca-Looping System for CO2 Capture. *Energy Fuels* **2012**, *26*, 1432-1440.
20. Yin, J.; Qin, C.; Feng, B.; Ge, L.; Luo, C.; Liu, W.; An, H., Calcium Looping for CO2 Capture at a Constant High Temperature. *Energy Fuels* **2013**, *28*, 307-318.
21. Rouchon, L.; Favergeon, L.; Pijolat, M., Analysis of the Kinetic Slowing Down During Carbonation of CaO by CO2. *J. Therm. Anal. Calorim.* **2013**, *113*, 1145-1155.
22. Butler, J. W.; Jim Lim, C.; Grace, J. R., Kinetics of CO2 Absorption by CaO through Pressure Swing Cycling. *Fuel* **2014**, *127*, 78-87.
23. Yin, J.; Kang, X.; Qin, C.; Feng, B.; Veeraragavan, A.; Saulov, D., Modeling of CaCO3 Decomposition under CO2/H2O Atmosphere in Calcium Looping Processes. *Fuel Process. Technol.* **2014**, *125*, 125-138.
24. Criado, Y. A.; Arias, B.; Abanades, J. C., Effect of the Carbonation Temperature on the CO2 Carrying Capacity of CaO. *Ind. Eng. Chem. Res.* **2018**, *57*, 12595-12599.
25. Arcenegui Troya, J. J.; Moreno, V.; Sanchez-Jimenez, P. E.; Perejon, A.; Valverde, J. M.; PerezMaqueda, L. A., Effect of Steam Injection During Carbonation on the Multicyclic Performance of Limestone (CaCO3) under Different Calcium Looping Conditions: A Comparative Study. *ACS Sustainable Chem. Eng.* **2022**, *10*, 850-859.
26. Li, Z.; Guo, X.; Xue, X.; Xu, X.; Wang, B., Investigations on Kinetics and Mechanisms of CaCO3 Calcination in Calcium Looping. *Ind. Eng. Chem. Res.* **2023**, *62*, 4851-4863.
27. Gallagher, P. K.; Johnson, D. W., The Effects of Sample Size and Heating Rate on the Kinetics of the Thermal Decomposition of CaCO3. *Thermochim. Acta* **1973**, *6*, 67-83.
28. Beruto, D.; Searcy, A. W., Use of the Langmuir Method for Kinetic Studies of Decomposition Reactions: Calcite (CaCO3). *J. Chem. Soc., Faraday Trans. 1* **1974**, *70*, 2145-2153.
29. Gallagher, P. K.; Johnson, D. W., Kinetics of the Thermal Decomposition of CaCO3 in CO2 and Some Observations on the Kinetic Compensation Effect. *Thermochim. Acta* **1976**, *14*, 255-261.
30. Searcy, A. W.; Beruto, D., Kinetics of Endothermic Decomposition Reactions. 2. Effects of the Solid and Gaseous Products. *J. Phys. Chem.* **1978**, *82*, 163-167.
31. Maciejewski, M.; Oswald, H. R., Morphological Observations on the Thermal Decomposition of Calcium Carbonate. *Thermochim. Acta* **1985**, *85*, 39-42.
32. Maciejewski, M.; Reller, A., How (Un)Reliable Are Kinetic Data of Reversible Solid-State Decomposition Processes? *Thermochim. Acta* **1987**, *110*, 145-152.
33. Criado, J.; González, M.; Málek, J.; Ortega, A., The Effect of the CO2 Pressure on the Thermal Decomposition Kinetics of Calcium Carbonate. *Thermochim. Acta* **1995**, *254*, 121-127.
34. Wang, Y.; Thomson, W. J., The Effects of Steam and Carbon Dioxide on Calcite Decomposition Using Dynamic X-Ray Diffraction. *Chem. Eng. Sci.* **1995**, *50*, 1373-1382.
35. Koga, N.; Criado, J. M., The Influence of Mass Transfer Phenomena on the Kinetic Analysis for the Thermal Decomposition of Calcium Carbonate by Constant Rate Thermal Analysis (CRTA) under Vacuum. *Int. J. Chem. Kinet.* **1998**, *30*, 737-744.
36. Rodriguez-Navarro, C.; Ruiz-Agudo, E.; Luque, A.; Rodriguez-Navarro, A. B.; Ortega-Huertas, M., Thermal Decomposition of Calcite: Mechanisms of Formation and Textural Evolution of CaO Nanocrystals. *Am. Mineral.* **2009**, *94*, 578-593.
37. Valverde, J. M.; Sanchez-Jimenez, P. E.; Perez-Maqueda, L. A., Limestone Calcination Nearby Equilibrium: Kinetics, CaO Crystal Structure, Sintering and Reactivity. *J. Phys. Chem. C* **2015**,*119*, 1623-1641.
38. Tsuboi, Y.; Koga, N., Thermal Decomposition of Biomineralized Calcium Carbonate: Correlation between the Thermal Behavior and Structural Characteristics of Avian Eggshell. *ACS Sustainable Chem. Eng.* **2018**, *6*, 5283-5295.

39. Tone, T.; Hotta, M.; Koga, N., Acceleration Effect of Atmospheric Water Vapor on the Thermal Decomposition of Calcium Carbonate: A Comparison of Various Resources and Kinetic Parameterizations. *ACS Sustainable Chem. Eng.* **2022**, *10*, 11273-11286.
40. Hotta, M.; Tone, T.; Favergeon, L.; Koga, N., Kinetic Parameterization of the Effects of Atmospheric and Self-Generated Carbon Dioxide on the Thermal Decomposition of Calcium Carbonate. *J. Phys. Chem. C* **2022**, *126*, 7880-7895.
41. Benton, A. F.; Drake, L. C., Kinetics of Reaction and Adsorption in the System Silver—Oxygen. *J. Am. Chem. Soc.* **1934**, *56*, 255-263.
42. Zawadzki, J.; Bretsznajder, S., Some Remarks on the Mechanism of Reactions of the Type: Solid=Solid + Gas. *Trans. Faraday Soc.* **1938**, *34*, 951-959.
43. Ingraham, T. R.; Marier, P., Kinetic Studies on the Thermal Decomposition of Calcium Carbonate. *Can. J. Chem. Eng.* **1963**, *41*, 170-173.
44. Barret, P., Expression théorique en Fonction de la Pression de la Loi de Vitesse de Croissance D'une Couche Non Protectrice Formée par Décomposition Thermique d'un Solide. *C. R. Acad. Sci. Paris, Serie C* **1968**, *266*, 856-859.
45. Reading, M.; Dollimore, D.; Whitehead, R., The Measurement of Meaningful Kinetic Parameters for Solid State Decomposition Reactions. *J. Therm. Anal.* **1991**, *37*, 2165-2188.
46. Deutsch, M.; Birkelbach, F.; Knoll, C.; Harasek, M.; Werner, A.; Winter, F., An Extension of the NPK Method to Include the Pressure Dependency of Solid State Reactions. *Thermochim.Acta* **2017**, *654*, 168-178.
47. Vyazovkin, S., Kinetic Effects of Pressure on Decomposition of Solids. *Int. Rev. Phys. Chem.* **2020**, *39*, 35-66.
48. Hariyadi, A.; Suwarno, S.; Denys, R. V.; von Colbe, J. B.; Sætre, T. O.; Yartys, V., Modeling of the Hydrogen Sorption Kinetics in an AB2 Laves Type Metal Hydride Alloy. *J. Alloys Compd.* **2022**, *893*, 162135.
49. Koga, N.; Favergeon, L.; Kodani, S., Impact of Atmospheric Water Vapor on the Thermal Decomposition of Calcium Hydroxide: A Universal Kinetic Approach to a Physico-Geometrical Consecutive Reaction in Solid-Gas Systems under Different Partial Pressures of Product Gas. *Phys. Chem. Chem. Phys.* **2019**, *21*, 11615-11632.
50. Fukuda, M.; Favergeon, L.; Koga, N., Universal Kinetic Description for Thermal Decomposition of Copper(II) Hydroxide over Different Water Vapor Pressures. *J. Phys. Chem. C* **2019**, *123*, 20903-20915.
51. Yamamoto, Y.; Favergeon, L.; Koga, N., Thermal Dehydration of Lithium Sulfate Monohydrate Revisited with Universal Kinetic Description over Different Temperatures and Atmospheric Water Vapor Pressures. *J. Phys. Chem. C* **2020**, *124*, 11960-11976.
52. Preturlan, J. G. D.; Vieille, L.; Quiligotti, S.; Favergeon, L., Kinetics and Mechanism of the Dehydration of Calcium Sulfate Dihydrate: A Comprehensive Approach for Studying the Dehydration of Ionic Hydrates under Controlled Temperature and Water Vapor Pressure. *J. Phys. Chem. C* **2020**, *124*, 26352-26367.
53. Koga, N.; Sakai, Y.; Fukuda, M.; Hara, D.; Tanaka, Y.; Favergeon, L., Universal Kinetics of the Thermal Decomposition of Synthetic Smithsonite over Different Atmospheric Conditions. *J. Phys. Chem. C* **2021**, *125*, 1384-1402.
54. Iwasaki, S.; Zushi, Y.; Koga, N., An Advanced Kinetic Approach to the Multistep Thermal Dehydration of Calcium Sulfate Dihydrate under Different Heating and Water Vapor Conditions: Kinetic Deconvolution and Universal Isoconversional Analyses. *Phys. Chem. Chem. Phys.* **2022**, *24*, 9492-9508.
55. Kodani, S.; Iwasaki, S.; Favergeon, L.; Koga, N., Revealing the Effect of Water Vapor Pressure on the Kinetics of Thermal Decomposition of Magnesium Hydroxide. *Phys. Chem. Chem. Phys.* **2020**, *22*, 13637-13649.
56. Sakai, Y.; Iwasaki, S.; Kikuchi, S.; Koga, N., Influence of Atmospheric CO2 on the Thermal Decomposition of Perlite Concrete. *J. Therm. Anal. Calorim.* **2022**, *147*, 5801-5813.

57. Sakai, Y.; Koga, N., Kinetics of Component Reactions in Calcium Looping Appeared During the Multistep Thermal Decomposition of Portland Cement under Various Atmospheric Conditions. *Chem. Eng. J.* **2022**, *428*, 131197.
58. Zushi, Y.; Iwasaki, S.; Koga, N., Effect of Atmospheric Water Vapor on Independent-Parallel Thermal Dehydration of a Compacted Composite of an Inorganic Hydrate: Sodium Carbonate Monohydrate Grains Comprising Crystalline Particles and a Matrix. *Phys. Chem. Chem. Phys.* **2022**, *24*, 29827-29840.
59. Koga, N.; Vyazovkin, S.; Burnham, A. K.; Favergeon, L.; Muravyev, N. V.; Pérez-Maqueda, L. A.; Saggese, C.; Sánchez-Jiménez, P. E., ICTAC Kinetics Committee Recommendations for Analysis of Thermal Decomposition Kinetics. *Thermochim. Acta* **2023**, *719*, 179384.
60. Vyazovkin, S.; Burnham, A. K.; Criado, J. M.; Pérez-Maqueda, L. A.; Popescu, C.; Sbirrazzuoli, N., ICTAC Kinetics Committee Recommendations for Performing Kinetic Computations on Thermal Analysis Data. *Thermochim. Acta* **2011**, *520*, 1-19.
61. Koga, N., Ozawa's Kinetic Method for Analyzing Thermoanalytical Curves. *J. Therm. Anal. Calorim.* **2013**, *113*, 1527-1541.
62. Koga, N.; Šesták, J.; Simon, P., Some Fundamental and Historical Aspects of Phenomenological Kinetics in the Solid State Studied by Thermal Analysis. In *Thermal Analysis of Micro, Nanoand Non-Crystalline Materials*, Šesták, J.; Simon, P., Eds. Springer: Dordrecht, 2013; pp 1-28.
63. Koga, N.; Tanaka, H., Effect of Sample Mass on the Kinetics of Thermal Decomposition of a Solid .2. Isothermal Dehydration of Li2SO4·H2O. *J. Therm. Anal.* **1993**, *40*, 1173-1179.
64. Vyazovkin, S.; Chrissafis, K.; Di Lorenzo, M. L.; Koga, N.; Pijolat, M.; Roduit, B.; Sbirrazzuoli, N.; Suñol, J. J., ICTAC Kinetics Committee Recommendations for Collecting Experimental Thermal Analysis Data for Kinetic Computations. *Thermochim. Acta* **2014**, *590*, 1-23.
65. Ogasawara, H.; Koga, N., Kinetic Modeling for Thermal Dehydration of Ferrous Oxalate Dihydrate Polymorphs: A Combined Model for Induction Period-Surface Reaction-Phase Boundary Reaction. *J. Phys. Chem. A* **2014**, *118*, 2401-2412.
66. Hotta, M.; Tone, T.; Koga, N., Effects of Particle Size on the Kinetics of Physico-Geometrical Consecutive Reactions in Solid–Gas Systems: Thermal Decomposition of Potassium Hydrogen Carbonate. *J. Phys. Chem. C* **2021**, *125*, 22023-22035.
67. Toft Sorensen, O. T.; Rouquerol, J., *Sample Controlled Thermal Analysis*; Kluwer: Dordrecht, 2003.
68. Criado, J. M.; Perez-Maqueda, L. A.; Koga, N., Sample Controlled Thermal Analysis (SCTA) as a Promising Tool for Kinetic Characterization of Solid-State Reaction and Controlled Material Synthesis. In *Thermal Physics and Thermal Analysis*, Šesták, J.; Hubík, P.; Mareš, J. J., Eds. Springer Nature: Switzerland, 2017; pp 11-43.
69. Koga, N., Thermoanalytical Methods: Fundamental Principles and Features. In *Thermal Analysis of Polymeric Materials: Methods and Developments*, Pielichowski, K.; Pielichowska, K., Eds. Wiley: Hoboken, NJ, 2022; pp 1-39.
70. Favergeon, L.; Morandini, J.; Pijolat, M.; Soustelle, M., A General Approach for Kinetic Modeling of Solid-Gas Reactions at Reactor Scale: Application to Kaolinite Dehydroxylation. *Oil Gas Sci. Technol.* **2013**, *68*, 1039-1048.
71. Iwasaki, S.; Zushi, Y.; Koga, N., Geometrical Constraints of Thermal Dehydration of β-Calcium Sulfate Hemihydrate Induced by Self-Generated Water Vapor. *Phys. Chem. Chem. Phys.* **2021**, *23*, 22972-22983.
72. Koga, N., Physico-Geometric Approach to the Kinetics of Overlapping Solid-State Reactions. In *Handbook of Thermal Analysis and Calorimetry*, 2nd ed.; Vyazovkin, S.; Koga, N.; Schick, C., Eds. Elsevier: Amsterdam, 2018; Vol. 6, pp 213-251.
73. Friedman, H. L., Kinetics of Thermal Degradation of Char-Forming Plastics from Thermogravimetry: Application to a Phenolic Plastic. *J. Polym. Sci., Part C* **1964**, *6*, 183-195.
74. Ozawa, T., Kinetic Analysis of Derivative Curves in Thermal Analysis. *J. Therm. Anal.* **1970**, *2*, 301-324.
75. Ozawa, T., Applicability of Friedman Plot. *J. Therm. Anal.* **1986**, *31*, 547-551.
76. Málek, J., The Kinetic Analysis of Non-Isothermal Data. *Thermochim. Acta* **1992**, *200*, 257-269.
77. Koga, N., Kinetic Analysis of Thermoanalytical Data by Extrapolating to Infinite Temperature. *Thermochim. Acta* **1995**, *258*, 145-159.

78. Gotor, F. J.; Criado, J. M.; Málek, J.; Koga, N., Kinetic Analysis of Solid-State Reactions: The Universality of Master Plots for Analyzing Isothermal and Nonisothermal Experiments. *J. Phys. Chem. A* **2000**, *104*, 10777-10782.
79. Criado, J. M.; Perez-Maqueda, L. A.; Gotor, F. J.; Málek, J.; Koga, N., A Unified Theory for the Kinetic Analysis of Solid State Reactions under Any Thermal Pathway. *J. Therm. Anal. Calorim.* **2003**, *72*, 901-906.
80. Ozawa, T., A New Method of Analyzing Thermogravimetric Data. *Bull. Chem. Soc. Jpn.* **1965**, *38*, 1881-1886.
81. Ozawa, T., Non-Isothermal Kinetics and Generalized Time. *Thermochim. Acta* **1986**, *100*, 109-118.
82. Šesták, J.; Berggren, G., Study of the Kinetics of the Mechanism of Solid-State Reactions at Increasing Temperatures. *Thermochim. Acta* **1971**, *3*, 1-12.
83. Šesták, J., Diagnostic Limits of Phenomenological Kinetic Models Introducing the Accommodation Function. *J. Therm. Anal.* **1990**, *36*, 1997-2007.
84. Šesták, J., Rationale and Fallacy of Thermoanalytical Kinetic Patterns. *J. Therm. Anal. Calorim.* **2011**, *110*, 5-16.
85. Spencer, W. D.; Topley, B., Cccliv.-Chemical Kinetics of the System Ag2CO3 ⇄ Ag2O + CO2. *J. Chem. Soc.* **1929**, 2633-2650.
86. Serris, E.; Favergeon, L.; Pijolat, M.; Soustelle, M.; Nortier, P.; Gärtner, R. S.; Chopin, T.; Habib, Z., Study of the Hydration of CaO Powder by Gas–Solid Reaction. *Cem. Concr. Res.* **2011**, *41*, 1078-1084.
87. Rouchon, L.; Favergeon, L.; Pijolat, M., New Kinetic Model for the Rapid Step of Calcium Oxide Carbonation by Carbon Dioxide. *J. Therm. Anal. Calorim.* **2013**, *116*, 1181-1188.
88. Liavitskaya, T.; Vyazovkin, S., Discovering the Kinetics of Thermal Decomposition During Continuous Cooling. *Phys. Chem. Chem. Phys.* **2016**, *18*, 32021-32030.
89. Liavitskaya, T.; Vyazovkin, S., Delving into the Kinetics of Reversible Thermal Decomposition of Solids Measured on Heating and Cooling. *J. Phys. Chem. C* **2017**, *121*, 15392-15401.
90. Yokokawa, H.; Yamauchi, S.; Matsumoto, T., The Thermodynamic Database MALT. *Calphad* **1999**, *23*, 357-364.
91. Yokokawa, H.; Yamauchi, S.; Matsumoto, T., Thermodynamic Database MALT for Windows with gem and CHD. *Calphad* **2002**, *26*, 155-166.
92. Favergeon, L.; Pijolat, M.; Soustelle, M., Surface Nucleation and Anisotropic Growth Models for Solid-State Reactions. *Thermochim. Acta* **2017**, *654*, 18-27.
93. Mampel, K. L., Time Conversion Formulas for Heterogeneous Reactions at the Phase Boundaries of Solid Bodies, I: The Development of the Mathematical Method and the Derivation of Area Conversion Formulas. *Z. Phys. Chem. Abt. A* **1940**, *187*, 43-57.